DIGITAL PROJECTION PHOTOCHEMICAL ETCHING FOR GRAY-SCALE SEMICONDUCTOR APPLICATIONS

BY

KAIYUAN WANG

THESIS

Submitted in partial fulfillment of the requirements
for the degree of Master of Science in Electrical and Computer Engineering
in the Graduate College of the
University of Illinois at Urbana-Champaign, 2014

Urbana, Illinois

Adviser:

Associate Professor Lynford L. Goddard

Abstract

In the contemporary semiconductor industry, with the ever-growing demand for smaller, denser, and newer device features, various industrial and academic research groups across the world are looking beyond the conventional planar lithography and fabrication methods for semiconductor materials. The rapidly evolving domain of 3-dimensional and gray-scale semiconductor device fabrication paves the way for a wide range of revolutionary techniques, innovative applications, and promising products.

This thesis presents digital projection photochemical etching, a novel and dynamic semiconductor fabrication technique that achieves a 3-dimensional structure in a single etch step. This technique utilizes a commercial digital projector to focus a substantially de-magnified image beam pattern onto the semiconductor sample, where the projected image itself is used to catalyze and define the etching. The discussion begins with a thorough introduction and literature review to cover the fundamental mechanisms behind the technique of photochemical etching. This is followed by an in-depth explanation of the methodology of experimental design and setup configuration. Subsequently, the thesis comprehensively describes the fabrication of various novel structures and devices using digital projection photochemical etching, demonstrating this technique's resolution, dynamics, and ability to integrate with higher-resolution lithography methods while preserving the unique gray-scale feature control.

Acknowledgments

I would like to express my sincere gratitude to my adviser, Prof. Lynford Goddard, for his inspirational guidance and support, and to graduate researchers Dr. Christopher Edwards, Lonna Edwards, and Dr. Xin Yu for providing their invaluable expertise and assistance.

Contents

Chapter 1. Introduction 1

1.1 Motivation 1

1.2 Current Research 1

1.3 Research Outline 3

Chapter 2. Literature Review 4

Chapter 3. Methodology 11

3.1 Experimental Setup 11

3.1.1 Physical Configuration 11

3.1.2 Chemical Recipe 14

3.2 Experimental Procedure 15

Chapter 4. Characterization Tests 17

4.1 Color Intensity Gradient Test 17

4.2 Temperature Test 19

4.3 Resolution Test 20

Chapter 5. Fabrication of High-Resolution Gray-Scale Structures 23

5.1 Integration with Photolithography 23

5.2 Integration with E-beam Lithography 26

Chapter 6. Fabrication of Gray-Scale Devices 29

6.1 Microfluidic Channel for Cell Differentiation 29

6.2 Variable-Height Pyramid Array for Sensing Applications 32

6.3 Waveguide Converter with Vertical Taper 34

Chapter 7. Conclusions and Future Work 38

References 40

Appendix A: Miscellaneous Fabricated Patterns 43

Appendix B: Digital Projection Photoelectrochemical Etching of Si 47

Appendix C: Digital Projection Photochemical Etching with Citric Acid 50

Chapter 1. Introduction

1.1 Motivation

The semiconductor industry has undergone a groundbreaking revolution since the mid-20th century following the invention of the integrated circuit and a wide range of patterning, deposition and processing techniques for semiconductor materials. In today's information age, a myriad of different integrated circuits, optoelectronic devices, and microelectronic systems play pivotal roles in almost all aspects of society. With the rapidly-expanding market of digital and mobile devices and gadgets, the growth of the microelectronics and semiconductor industries shows no sign of slowing down.

As a result, governed by the famous Moore's law, the demand for more intricate and sophisticated device features has been greater than ever, even accounting for the radical improvements of device size and complexity over the past few decades. This growing and diversifying demand magnifies the limitations of conventional planar lithographic patterning techniques, and draws attention to the novel fabrication techniques for 3-dimensional semiconductor structures and devices.

With 3-dimensional patterning capabilities, control and manipulation in one additional dimension drastically broaden the horizon for countless new device designs and functional possibilities. However, better resolution, higher throughput, and lower cost have been some of the biggest impediments for most of the existing 3-dimensional patterning methods [1-3]. They are also the top priorities for improvement for many industrial and academic research groups focusing on 3-dimensional and gray-scale semiconductor fabrication methods. The next section evaluates existing industrial technologies for 3-dimensional patterning of semiconductor materials. This will provide a few relevant parameters of comparison during the subsequent presentation of digital projection photochemical etching, a promising technique for gray-scale topographical control during semiconductor fabrication and processing.

1.2 Current Research

There have been substantial developments utilizing many different mechanisms for 3-dimensional semiconductor fabrication over the past three decades. The first major class of techniques utilizes 3-

dimensional lithography to spatially define polymers and photoresists, such as stereolithography, multiphoton lithography, direct laser lithography, and nanoimprint lithography. A major limitation of these 3-dimensional lithography techniques is that they are generally applied on a photo-polymer material [4]. As these patterning techniques are generally not directly effective on semiconductor substrates, the pattern on the photoresist that is spatially-varied in all three dimensions could only be transferred to the semiconductor substrate through an additional process [5]. For example, during an additional etching step, the dissolution of the patterned photoresist polymer will expose the substrate surface gradually and result in differential etch times across different regions of the substrate surface, resulting in a 3-dimensional topography.

Secondly, another major class of 3-dimensional fabrication utilizes a direct-etching mechanism. This includes various wet and dry processing techniques such as reactive-ion etching, plasma etching, Bosch process, and dose-controlled electron-beam lithography [6]. Such etching processes would often involve multiple mask patterning and etching steps to define the desired feature that is spatially varied in all three dimensions [7]. One major drawback of this mechanism is the need of multiple masks for the multiple pattern layers, which will be both time-consuming and expensive.

Thirdly, instead of etching from the wafer surface, there have been developments with controlled material growth on the surface of a semiconductor substrate. Various deposition mechanisms such as chemical vapor deposition (CVD) have been used to fabricate quantum wires, quantum dots, and other intricate features [8]. However, the topography of the structures fabricated through this mechanism is often limited to fundamental geometrical shapes. Although the deposition and growth mechanism implements very small quantum confined device features, precise gray-scale depth control across a large area of the substrate surface will require highly complicated monitoring and time-consuming multi-step implementation.

After considering some of the conventional mechanisms for 3-dimensional semiconductor structure fabrication, it is notable that these techniques usually require costly equipment and lengthy processing to fabricate the 3-dimensional or gray-scale features. The next section will elucidate the research outline for the investigation of the gray-scale digital projection photochemical etching technique. It will be helpful to keep the conventional mechanisms and their traits in mind as a comparison throughout the discussion.

1.3 Research Outline

The investigation for the unique maskless digital projection photochemical etching will be holistically manifested in the design, fabrication, and refinement processes. The research outline includes recipe development, setup configuration, performance characterization, structure design, process integration, and device fabrication and testing.

The recipe development has been discussed in previous works [9], and would require less emphasis in the discussion. Since the setup configuration will be built from scratch, this requires meticulous alignment, characterization, and constant modification to the setup components and design. This construction process will be juxtaposed with a series of characterization tests for the evaluation of process performance and reliability, including factors such as spatial resolution, effects of color intensity and temperature. After settling on a sufficiently optimal system, trials at integration with conventional high-resolution lithography techniques will be investigated. Lastly, fabrication of several functional device prototypes will be carried out.

Chapter 2. Literature Review

The idea of light-catalyzed semiconductor etching has been evident in a wide range of research applications [10-14]. Although catalyzing a semiconductor etching reaction with light beam from a commercial projector is a relatively new concept that has yet to be widely investigated, it is still important to analyze the spectrum of past applications in the field of photochemical etching. The collection of relevant past research results and experiences could be utilized in the current and future research design and implementation.

In this chapter, a critical review and analysis of numerous representative examples directly relevant to the research investigation is carried out. By evaluating these approaches comparable to the current research methodology, potential improvements and modifications could be achieved. The subsequent literature review case studies are arranged chronologically by publication date.

Carrier-lifetime-controlled selective etching process for semiconductors (1989) [15]

This patent explained how decreasing minority carrier life-time through increasing the impurity concentrations permits highly selective semiconductor material etching. A carrier-driven photochemical etching reaction is achieved through manipulation of the carrier life-time. Given that the etching process requires direct participation of electronic charge carriers, it is significantly influenced by light absorption in the semiconductor material, which subsequently dictates the etch rate of the material. Various mechanisms such as localized impurity increase could be implemented to influence the impurity concentration level across the surface and thus create a variable wet etching process over different regions.

Electronic-carrier-controlled photochemical etching process in semiconductor (1989) [16]

This patent demonstrated an electronic-carrier-controlled photochemical etching process to selectively pattern and remove material in semiconductor device fabrication. It formulates the set of sequential steps for selective ion implanting, photochemical dry etching, and thermal annealing, as part of the fabrication process. There are a number of relevant takeaways regarding practices on patterning and selectively removing material through photochemical dry etching, where ion-implanted regions form the surface structures on the material surface at the end of the etching step.

Photochemical Etching of GaAs using Synchrotron Radiation (1990) [17]

A set of experiments was conducted to investigate the photochemical etching of GaAs by chlorine through synchrotron radiation. Varying temperature was presented as the main factor to be analyzed. Different etch rates and performances were observed at different temperatures ranging from below -25 °C to above 25 °C. A low-temperature environment was postulated to have caused the suppression of etching reaction by gas-phase excitation, leading to a domination of the photochemical surface reaction. While the mechanisms discussed in this case might be different from the digital projection photochemical etching technique, the influence of temperature and external environmental factors could be significant variables to keep in mind for the current experiments.

Photochemical etching of n-lnP as a function of temperature and illumination (1990) [13]

This paper investigated n-InP photochemical etching with Ar+ laser and dilute phosphoric acid solutions. This demonstrates how variables such as temperature, power, illumination frequency and duty cycle affect the etching process. It was discovered that temperature and power affect the etch rate significantly, leading to a fourfold etch rate increase for a temperature increase from 20 °C to 50 °C. In addition, with power at the low-power range, the etch rate increased and saturated at an irradiance of 200 W/cm^2 at around 20 °C.

The effect of temperature and power on the etch rate is heavily relevant to the current investigation of etch performances. A similar approach has been utilized in the current experimental procedures to study the etch resolution and etch rate versus projector color wavelength and intensity. Furthermore, this paper also presented discussions on the effects of illumination duty cycle, rate equation model for material removal, and sample preparation for transmission electron microscopy as an uncommon application of photochemical etching.

Laser projection patterned etching of GaAs in a chlorine atmosphere (1992) [18]

This set of experiments explored the etching of GaAs in chlorine, which was carried out through the formation and subsequent evaporation of gallium and arsenic chlorides, a process facilitated with a pulsed KrF excimer laser (λ=248 nm, τ=15 ns) and deep ultraviolet projection optics. Projection-patterned etching of GaAs has been achieved with a resolution down to the optical resolution of the projection system at 2 μm. While this etching process is broadly different from the current photochemical etching

mechanism under investigation, it is nevertheless applicable in aspects of characterization principles such as resolution tests.

Pattern formation techniques in photochemical etching (1992) [19]

In this investigation, the major techniques of pattern formation in photochemical etching were comprehensively discussed. The methods evaluated are image projection, contact or proximity masking, direct writing, optical (holographic) interference, and patterned pre-etch substrate modification. Specifically, the method of image projection discussed here uses a mask, situated remotely from the substrate surface, to create an image pattern which will be demagnified by projection optics before focusing at the material surface. The digital projection approach taken in the current research replaces the physical mask with a digital image, greatly simplifying the process. It was stated that the usefulness of each method for a specific purpose will be determined by both the inherent optical properties of the pattern-forming technique, and the chemical and physical characteristics of the specific etching process.

This paper presented a thorough introduction of the orthodox photochemical etching mechanisms. Specifically, the discussion listed a few optical characterization approaches for the direct optical writing mechanism, which will be most relevant with respect to the current digital projection photochemical etching. The related principles would include the Gaussian profile of the light beam, the dependence on temperature, and the possible degradation of resolution due to the ripple effect in the projected image. These factors could be prudently incorporated in the methodology of the current research plans.

Photochemical etching of n-lnP: Observations on photon efficiency and saturation (1993) [20]

The photochemical etching of n-InP in dilute phosphoric acid was characterized in this paper. The effects and observations on photon efficiency and saturation were investigated. For the etching process, the experiment utilized an Argon laser with a wavelength of 488 nm. Experimental results on the etch rate performance as affected by duty cycle and frequency were evaluated, representing a few potential implications for maskless photochemical etching and semiconductor processing. A decrease in duty cycle was shown to increase the illumination etch rate, providing a few relevant parameters which could be incorporated into the current investigation involving digital projection photochemical etching. Also, experimental design for the current research setup involving optical projectors could potentially adapt the applicable analysis of duty cycle as a variable that affects the etch rate; this will possibly be dependent on the light projection mechanism of the optical projector.

Guide to references on III-V semiconductor chemical etching (2001) [21]

This comprehensive publication covered in detail the etching recipes for the light-catalyzed wet etching of GaAs. The etch recipes generally consist of an acid (e.g. H_2SO_4, H_3PO_4), an oxidizer (e.g. H_2O_2, $KMnO_3$), and water as a diluent. It will be useful to experiment with the chemical combinations proposed in this paper to obtain recipes that are either selective or non-selective for GaAs over other semiconductor materials such as AlGaAs, and vice versa. This could potentially be repeated with GaAs versus a wide range of other compounds, possibly summarizing the results in a table to facilitate future investigations.

Laser-induced etching of CrO doped GaAs and wavelength dependent photoluminescence (2004) [22]

In this paper, the laser-induced etching of GaAs with CrO doping was explained with the generation of electron-hole pairs through defect states in the presence of sub-bandgap photon illumination using a Nd:YAG laser. These surface defect states would be responsible for the formation of pitted structures within the GaAs substrate, serving as a worthwhile comparison with investigations on the current photochemical etching process.

Direct patterning of silicon by photoelectrochemical etching (2005) [23]

This patent made use of a resistless projection lithographic method which concurs greatly with the concept of digital projection photochemical etching, except for the addition of voltage bias across the wafer sample and the surrounding etchant. It was stated that a porous silicon structure had been created from this etching process and the removal of the porous silicon layer left a 3-dimensional structure characterized by the projected optical pattern. Through a comparison of the smallest feature size achieved, the current gray-scale digital projection photochemical etching technique significantly outmatches this reported method, in which a minimum feature size of 70 μm had been demonstrated. It is useful to keep in mind the effect of doping on the resolution of features attainable, as better results are possible with variation in doping of the substrate material.

Sulfidic photochemical passivation of GaAs surfaces in alcoholic solutions (2005) [24]

This article investigated the sulfidic photochemical passivation of GaAs surfaces in alcoholic solutions. A significant improvement of the passivation effect of sulfidic solutions through illumination was reported, with photoelectron spectroscopy determining that the illumination led to a removal of surface oxides. This investigation represents a possible spin-off from the present investigation of GaAs photochemical etching processes, presenting a different area in which photochemical etching could be

utilized. It is useful to consider that the photochemically-passivated semiconductor has a decreased extent of band-bending and depinning of the Fermi-level for the GaAs material, which could be incorporated in various fundamental semiconductor applications such as Schottky diodes.

Photo-selective chemical etching of InAs and GaSb to manufacture microscopic mirrors (2008) [25]

This study asserted that there was a renewed interest in photochemical processing due to the developments and demands in various micro-electro-mechanical systems (MEMS) and optoelectronic applications, such as light-emitting diodes and lasers with integrated lenses or gratings. This article explained a photo-selective chemical etching method for microscopic mirror manufacturing, also known as the Laser-Assisted Chemical Etching (LACE) technique. A beam of monochromatic photons was projected through the laser, leading to an active control of reactive interactions near the surfaces of the InAs and GaSb semiconductor material surface. This controlled etching process enabled the relatively localized etching without intermediate mask assistance, and was applied to n-type GaSb substrates to create cavities with nearly parabolic cross-sectioned profiles. The group demonstrated near-parabolic cavities on GaSb structures that could be used as micro-mirrors or micro-lenses, and opened up possibilities of fabricating mono-mode unstable cavities for optoelectronic devices such as the vertical cavity surface emitting lasers (VCSELs). As such, this paper contains many beam and pattern manipulation approaches for the light-catalyzed wet etching process, and would be hugely relevant to the subsequent device design and fabrication analysis.

Size-selective laser-induced etching of semi-insulating GaAs: Photoluminescence studies (2009) [26]

This article discussed the size-selective laser-induced etching of GaAs, creating a porous structure through manipulating the exposure time. The etch-time dependent photoluminescence spectroscopy results demonstrated that direct tuning of the nano-crystallite size was limited by oxide layer formation on the substrate surface. A relevant discussion on imaging processes using atomic force microscopy (AFM) and scanning electron microscopy (SEM) was also conducted. This investigation provided a few purposeful insights on the effect of etch duration and surface reactions on GaAs substrates during the etching process.

Formation of high aspect ratio GaAs nanostructures with metal-assisted chemical etching (2011) [27]

Periodic high-aspect-ratio GaAs nano-pillars with widths in the range of 500–1000 nm were produced by a mechanism called metal-assisted chemical etching (MacEtch), using n-type (100) GaAs

substrates and Au catalyst films patterned with soft lithography. The n-type GaAs wafers, patterned by Au, are etched using soft lithography with $KMnO_4$ as the oxidizing agent in acidic (H_2SO_4 or HF) solutions, demonstrating that ordered arrays of high aspect ratio GaAs nanostructures can be formed using Au-MacEtch. This series of research work on high aspect ratio structures is analogous to light-catalyzed photochemical etching, sharing the same concept of utilizing active carriers for a catalyzed surface etching process on semiconductor materials.

Optically monitoring and controlling nanoscale topography during semiconductor etching (2012) [10]

This highly relevant article presented epi-diffraction phase microscopy (epi-DPM) as a non-destructive optical method for monitoring semiconductor fabrication processes. It also contains detailed documentation on the concurrent use of digital projection photochemical etching to fabricate samples for the epi-DPM imaging process. An in-depth analysis for the field-of-view of the projected image was carried out. In addition, this article also presented various data manipulation and analysis methods to reduce the noise and curvature of the results collected. Furthermore, various images of the etched micro-pillars were presented and the sequential specifics of the process were recorded, including the collection of a three-dimensional movie showing the dynamics of the wet etching process. This investigation provided the essential framework for the current research on gray-scale digital projection photochemical etching.

Digital projection photochemical etching defines gray-scale features (2013) [9]

This article documented the essential methodology and research results of the digital projection photochemical etching hitherto, providing a foundation for the current experimental design and implementation. In this paper, the maskless photochemical etching method capable of fabricating any arbitrary gray-scale feature in a single etch step was demonstrated. This method utilized a digital projector to focus a de-magnified image onto GaAs substrate samples, delineating the gray-scale etch pattern in a wet etch with dilute phosphoric acid and hydrogen peroxide etchant. Measurements of etch features were conducted using the diffraction phase microscopy (DPM) imaging method in a non-destructive manner. A study on the etch rate as a function of the wavelength and irradiance of the projected light was implemented. It was determined that the lateral etch resolution is around 2 μm, as demonstrated by etching selected portions of the USAF-1951 target. In addition, various gray-scale features were fabricated and imaged, including micropillars, multi-level plateaus, and an Archimedean spiral, to illustrate the unique capabilities of the digital projection photochemical etching technique.

Fabrication of diffractive optical elements with digital projection photochemical etching (2014) [28]

This paper represents a continuation of the discussion on digital projection photochemical etching following the previous article. In this article, digital projection photochemical etching was presented as a low-cost and dynamic fabrication technique for photonic devices such as diffractive optical elements. A radial sinusoidal grating is a new type of device that was fabricated using a projected gray-scale digital image mask. The resulting diffraction pattern was also analyzed to demonstrate the quality of the fabricated diffractive optical elements.

Chapter 3. Methodology

This chapter discusses the methodology of experimental setup and experimental procedures. The optimization process of various hardware specifications, optical element alignments, and other setup configurations will be enunciated. A complete documentation of the etching process will be outlined. Most, if not all, of the subsequent fabrication experiments will be based on the discussions in this chapter, accomplishing a reliable and efficient fabrication performance for the unique gray-scale capabilities.

3.1 Experimental Setup

3.1.1 Physical Configuration

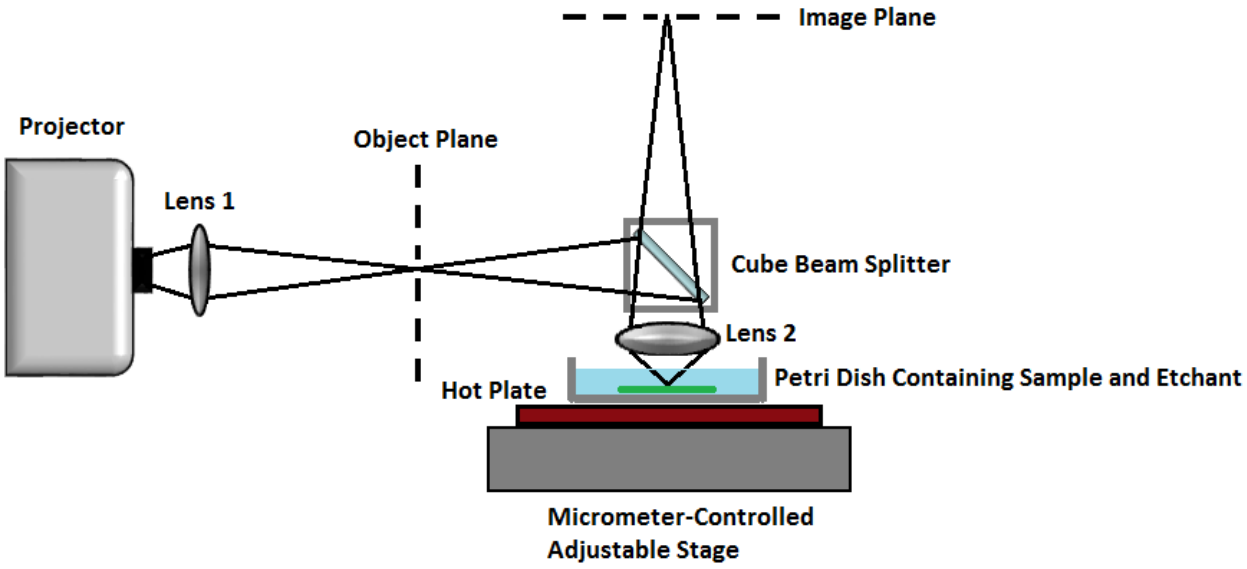

Figure 3.1: Experimental setup for digital projection photochemical etching.

Figure 3.1 succinctly illustrates the experimental configuration for digital projection photochemical etching. The projector, digitally connected to a computer via a video graphics array (VGA) cable, takes the input screen from the computer and projects the standard high-definition (1920 pixels wide and 1080 pixels tall) image as the optical output. The projector used for this experiment is an entry-level commercial projector for home, small office, and classroom use. The specifications of the projector are listed in Table 3.1. In addition, Figure 3.2 captures a front view of the ViewSonic PJD7820HD projector used in the experiments. The projector utilizes the digital light processing (DLP) technology in which the projected image is created by a matrix of microscopically small mirrors known as the digital micromirror device

(DMD). Each micromirror represents one pixel in the projected image, with the colors determined by a color wheel placed between the lamp and the DMD.

Table 3.1: Specifications for the projector used in the setup.

Brand	ViewSonic
Model	PJD7820HD
Type	0.65” Digital Micromirror Device (DLP)
Lens	1.3x manual optical zoom / manual optical focus
Keystone	Manual vertical digital keystone correction (+/- 40°)
Display size	30 – 300 in. / 0.7 – 7.6 m (diagonal)
Lamp type	210 Watt
Luminous flux	3,000 ANSI lumens
Contrast ratio	15,000:1
Resolution	1080p
Aspect Ratio	16:9
Color Wheel	6-seg RGBCYW / 7200rpm
Additional features	• 120Hz refresh rate with digital light processing • 3D Blu-ray ready with HDMI • 6-segment color wheel design • Lamp life up to 6,000 hours • Compatible with PC for VGA to full HD output • 260W power consumption • Net weight of 4.6 lbs. / 2.1 kg

Figure 3.2: Front view of the ViewSonic PJD7820HD Projector.

With reference to Figure 3.1, a convex lens pair collectively labeled as Lens 1, with an effective focal length of about 66.7 mm, is placed directly in front of the projector output. The purpose of this optical element is to collect the divergent beam image from the projector and create a small, clear, and focused projected image at Object Plane as marked, while remaining considerably collimated to be captured by the Cube Beam Splitter, specifically the CM1-BS013 30mm Cage Cube-Mounted Non-Polarizing Beamsplitter, 400-700 nm.

Tracing the beam direction from the Projector to the Cube Beam Splitter, the 50:50 beam splitter reflects exactly half of the light beam downwards, while the other half of the light beam that passes through will be inconsequential. The reflected beam passes through Lens 2, a 25mm-focal-length camera lens, which substantially shrinks the image beam and focuses the image onto the surface of the semiconductor sample, through a shallow layer of liquid etchant.

In order to accurately measure and observe the quality of the focused image on the sample, it will require an additional image plane to determine the uniformity and clarify of the projected image pattern. This is captured at the Image Plane above the beam splitter, which is formed by the reflected image beam from the surface of the sample, going back through Lens 2 and Cube Beam Splitter. The simple installation of a clean and smooth white screen at Image Plane enables characterization of the image, through direct observation visible to the naked eye.

Next, the position of the sample can be adjusted by motorized micrometers, which give precise control in all three dimensions. The micrometer controller is connected to a computer and can be manipulated using custom LabVIEW code. Furthermore, a digitally-controlled hotplate is positioned

directly below the petri dish containing the sample and etchant, adding precise temperature adjustment and control for the reaction conditions.

3.1.2 Chemical Recipe

The photochemical etching process was predominantly carried out on cleaved n+ GaAs (100) wafers using a diluted mixture of phosphoric acid and hydrogen peroxide, with specific concentrations of 1:1:50 of H_3PO_4:H_2O_2:H_2O. This specific combination of acid and oxidizer has been shown in past studies to provide stable etching and excellent reproducibility [29]. Regular 4-inch wafers are cleaved into small pieces of roughly 0.5 cm x 0.5 cm in area and placed in a small glass petri dish for etching. The amount of etchant used for each etch could vary, but is mostly standardized at 10 mL.

The specific chemistry of the reaction begins with an oxidation reaction were the hydrogen peroxide oxidizes the GaAs. Through the oxidation reaction of the arsenide ions with hydrogen peroxide, arsenic is oxidized to form the soluble oxide, As_2O_3, as shown by Equation (3.1). The gallium ions in GaAs are already fully oxidized in their Ga^{3+} state, forming the hydroxide $Ga(OH)_3$ as shown by Equation (3.2). Ga_2O_3 will be formed via the hydroxide, leading to a removal of the surface oxides as both As_2O_3 and Ga_2O_3 are soluble in phosphoric acid solutions, completing the corrosive process [30].

$$2\,As^{3-} + 6\,H_2O_2 + H^+ \rightarrow As_2O_3 + 5\,OH^- + 4\,H_2O \tag{3.1}$$

$$2\,Ga^{3+} + 6\,OH^- \rightarrow 2\,Ga(OH)_3 + 3\,H_2O \tag{3.2}$$

As light is shone on the substrate surface, photon absorption in the semiconductor material increases the concentration of excited electrons as minority carriers at the surface of the wafer sample, thus increasing the rate of dissolution and corrosion of the GaAs material in the etchant solution. Depending on whether the solution is diffusion or reaction limited, the acid to oxidizer ratio affects the etch rates and the surface roughness of etched features. Deionized water is used as a diluent, which contributes to the minimization of the dark background etch rate at low environmental light intensities.

3.2 Experimental Procedure

With reference to Figure 3.1:

(1) Mix Etchant:

H_3PO_4:H_2O_2:H_2O (1:1:50)

Volume of 3 mL, 3 mL, and 150 mL respectively

Mix with magnetic stirrer for 40 minutes

(2) Initial Alignment:

Turn on the Projector to display the image beam

Use dummy sample in petri dish with 10 mL of de-ionized water

Adjust stage position for optimal focus of physical sample plane as observed at Image Plane

Manipulate position of Projector and Lens 1 for simultaneous optimal focus of projected image

Lock position of optical elements for reproducibility in subsequent experiments

(3) Etching Preparation:

Turn on the Projector to display the image beam

Shake etchant for 1 minute

Place 10 mL of pre-mixed etchant in petri dish

Optional: turn on Hot Plate, heat the petri dish and etchant to the desired temperature

Turn off ambient light

Carefully place GaAs sample in the petri dish

Gently position the petri dish under Lens 2 on the Hot Plate

(4) Etching:

Move the petri dish slightly to align the light beam on the GaAs sample

Immediately fine-tune the focus using the micrometer, start timing

After desired etch time is reached, block / turn off the projector beam

Immediately remove and rinse the sample with de-ionized water thoroughly

Gently dry with N_2 gun or cleanroom wipes

Sample is ready for imaging

Repeat steps (3) and (4) for multiple etches

(5) Cleanup:

When finished, dispose of the etchants safely

Clean all the apparatus and glassware

Turn off all equipment

Chapter 4. Characterization Tests

A precise and accurate characterization of the digital projection photochemical etching technique is pivotal in providing a solid fundamental basis for any further attempts at device design and fabrication. As such, a series of characterization tests for factors such as color, intensity, and temperature are meticulously conducted and analyzed to optimize the fabrication process for ideal performances in resolution, etch rate, and surface smoothness.

4.1 Color Intensity Gradient Test

An exhaustive study was carried out on how the three fundamental colors of red, green, and blue at different color intensities dictate the etching process. This will be crucial for determining the relationship between the digitalized color intensities, on a standard RGB scale of 0 – 255, and the etch rate at a specific combination of RGB values. The successful implementation of advanced mask design for future device fabrication will be heavily dependent on this set of data. Figure 4.1 illustrates the full-HD resolution mask image design for the color intensity gradient test.

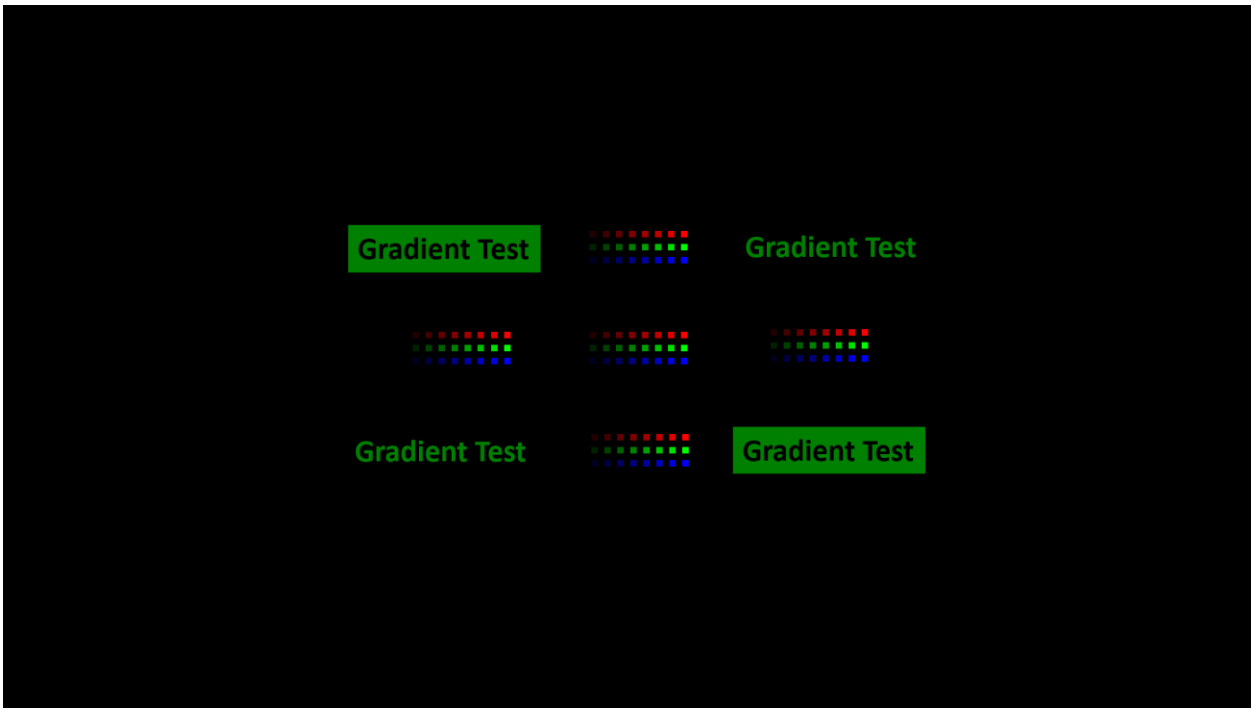

Figure 4.1: Mask image for the color intensity gradient test.

With reference to Figure 4.1, five sets of color and intensity spectra are spatially spread out across the center region of the projected image. Each set contains 8 squares for each of the red, green, and blue intensity spectrum, with a total of 24 squares in each set. The 8 squares are of respective RGB intensities 32, 64, 96, 128, 160, 192, 224, and 255, as shown from left to right. The texts in the background are used to facilitate focus optimization during alignment. Green is arbitrarily chosen for a balance between short wavelength and favorable visibility. A 15-second etch is carried out at room temperature of 23°C with the image mask focused onto a GaAs sample immersed in 10 mL of etchant. Various images and profile of the fabricated sample captured by optical microscope and DPM are collectively shown as Figure 4.2.

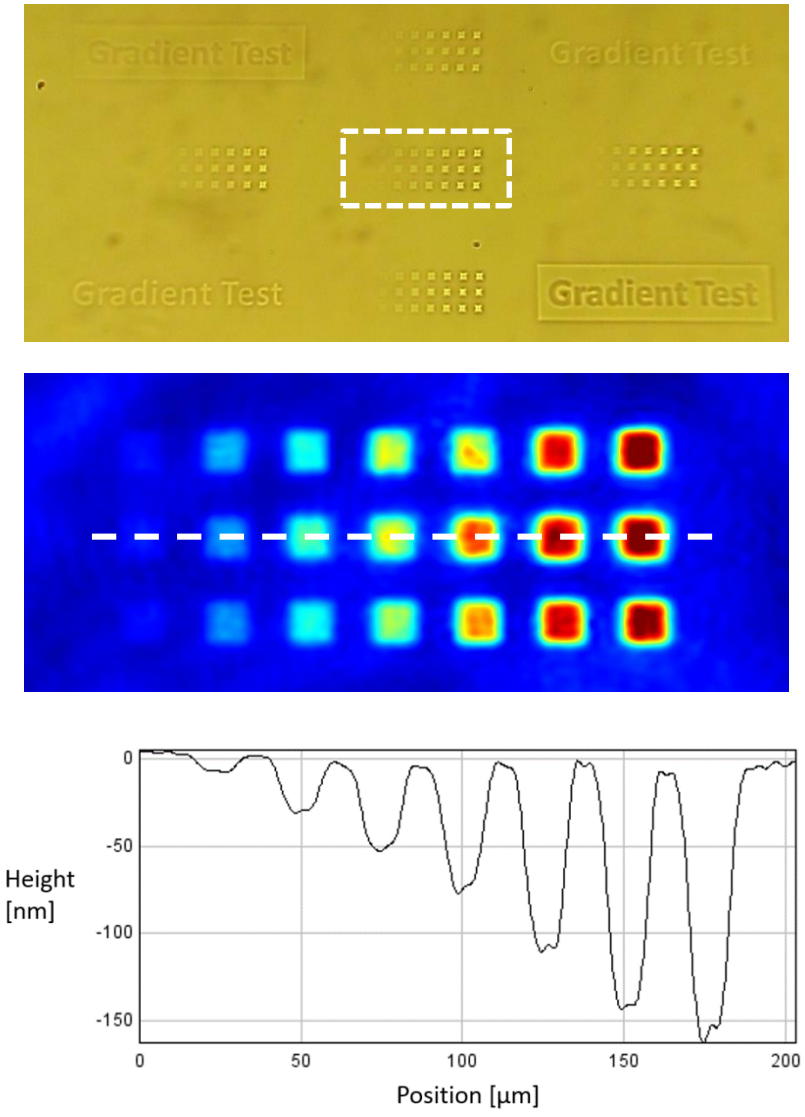

Figure 4.2: Optical-microscopy (top) and DPM (middle) images with cross-sectional profile (bottom) of the fabricated color intensity gradient sample. Magnified area and cross sectional profile are indicated by the dotted lines.

As observed in Figure 4.2, Green probably produced the most uniform etch patterns. The width of the Green intensity spectrum with 7 visible squares is approximately 180 µm. A preliminary calculation using the distance of 180 µm and a pixel count of 130 pixels in the digital mask image indicated that each side of the square pixel from the projected pattern is approximately 180 µm / 130 pixels ≈ 1.4 µm/pixel. In addition, the etch depth at a color intensity of 128 Green is 50 nm, leading to a differential etch rate of 50 nm / 15 sec ≈ 3.3 nm/sec. An inspection across the multiple sets of etch structures demonstrated that Green 128 would be a suitable color intensity to produce a reasonably stable etch rate and uniformity. However, it is necessary to note that the exact etch performance will be heavily influenced by pattern area, shape, and complexity. As such, Green 128 is tentatively selected as the default color intensity for subsequent characterization tests involving temperature and resolution.

4.2 Temperature Test

The next phase of the characterization tests investigated the effect of varying temperature on etch rate and uniformity. Using the same image mask from Figure 4.1, two more samples were each etched for 15 seconds at temperatures of 45 and 65 °C respectively. Surprisingly, after comparing these two samples with the sample from room-temperature etching in the previous section, it seems that changing the temperature did not have a conclusive visible effect on the etch rate and uniformity. This could be due to the short etch duration and the relatively small temperature variation range which was limited by the safety concerns in the laboratory. The optical microscopy images and profiles for the two samples fabricated at 45 and 65 °C are shown in Figure 4.3. The resolution and etch rate remain largely unchanged. There are small variations in the etch uniformity, but the discrepancies are insufficient to derive any discernable pattern. There is some variation in the shape of the etched trench. In comparing Figure 4.2 and 4.3, the lower temperature does seem to produce a flatter base of the trench.

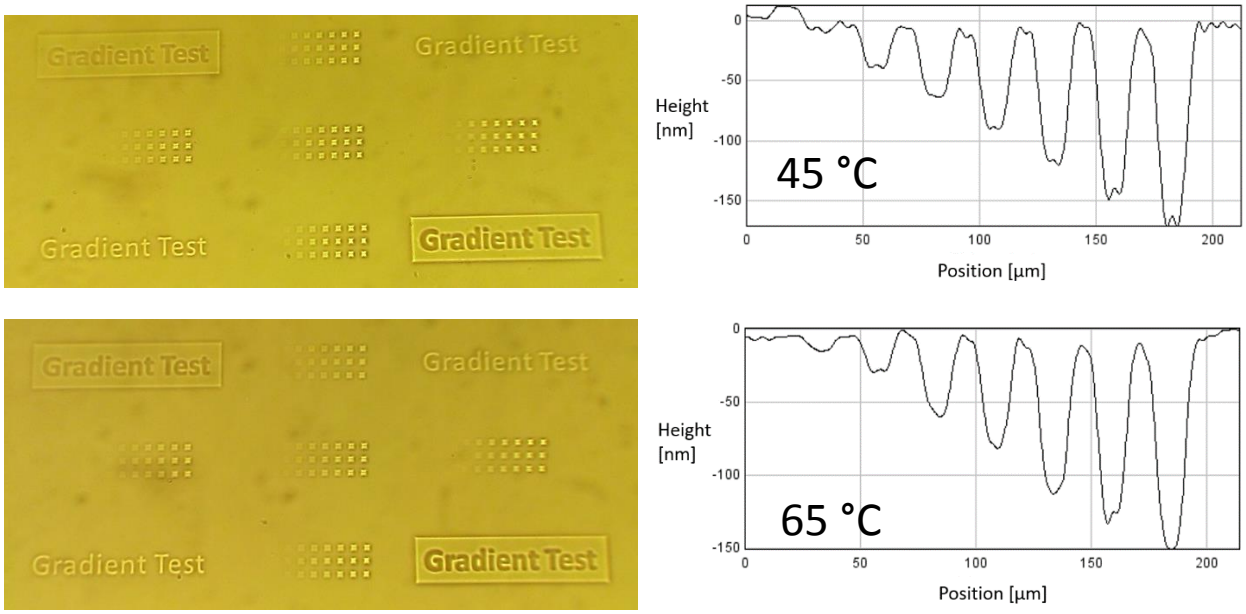

Figure 4.3: Optical microscopy images and cross-sectional profiles of the fabricated samples at 45 (top) and 65 (bottom) °C respectively. Cross-sectional profiles are obtained from the Green color-intensity spectrum at the center of the sample.

4.3 Resolution Test

The last critical phase of the characterization tests seeks to demonstrate the resolution of the digital projection photochemical etching technique in the current configuration. In an attempt to obtain the smallest resolvable feature possible, a sophisticated digital mask image for the resolution test is designed, as shown in Figure 4.4. In this resolution mask, two crosses with line thickness of 1 pixel are overlapped with a one-pixel incremental displacement from each other in both the x and y directions, as indicated by the numbers 0-7. A pair of positively and negatively-toned images are created for each of the 8 displacement values. With reference to the results from Section 4.1, each square pixel is approximately 1.4 µm by 1.4 µm.

The resolution mask is projected and the sample is etched for 30 seconds. Figure 4.5 presents the DPM image of the resulting etched patterns. While crosshair 3 was clearly resolvable, the image for crosshair 2 was not convincing. As such, a resolution of 3*1.4 µm = 4.2 µm can be conclusively demonstrated.

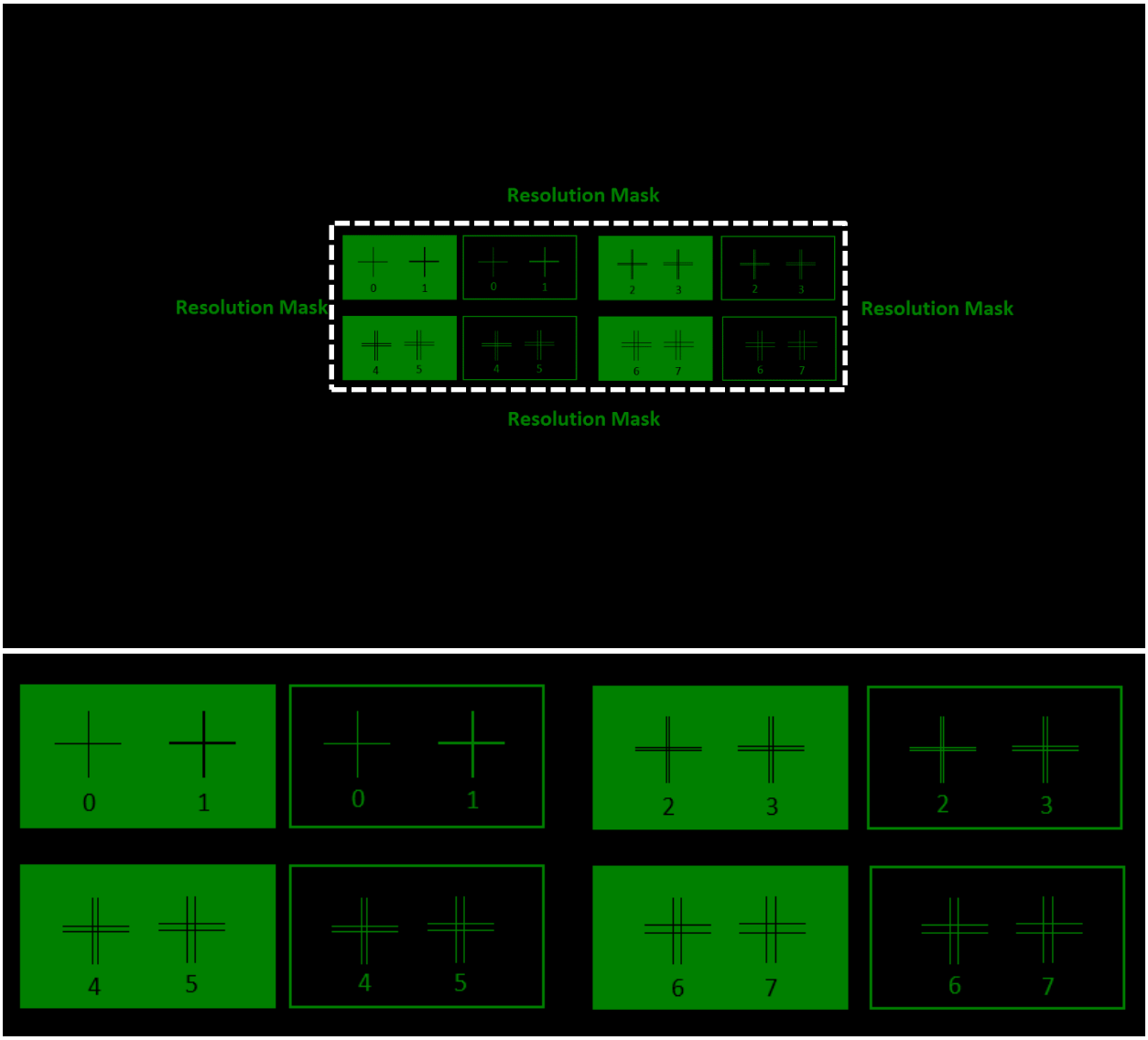

Figure 4.4: Full display of the resolution mask (top) and a magnified image of the features (bottom) as indicated by the dotted line.

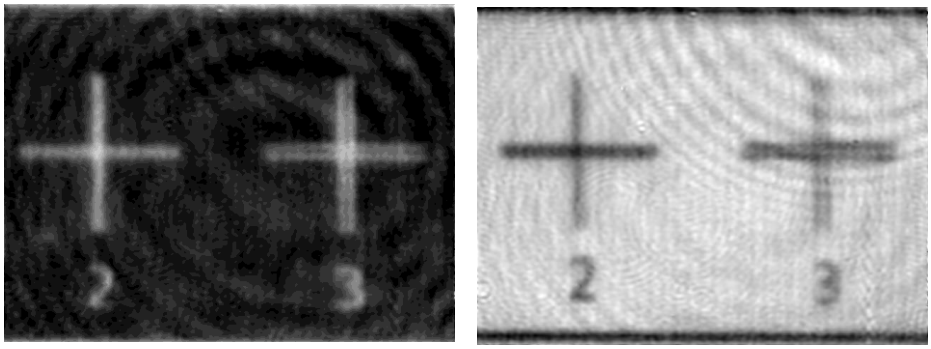

Figure 4.5: DPM images of the fabricated resolution mask patterns.

According to Abbe's formula, the resolution is proportional to the wavelength of the imaging radiation, and inversely proportional to the numerical aperture. The etching resolution for the digital projection photochemical etching is dictated by three factors. Firstly, the pixel size as characterized by the optical configuration will set a limit on the smallest feature resolvable. It is possible to improve the pixel size of 1.4 μm/pixel in the current configuration with optical elements of higher performance specifications. In addition, the improvements in optical elements such as projector, lens system, and control stage will reduce chromatic aberrations and non-uniformity from alignment imperfections. Secondly, with reference to Abbe's formula, there is a diffraction limit of the visible light used in etching. Visible light from a digital projector exhibits a wavelength spectrum of about 750 – 380 nm, which will intrinsically limit the resolution obtainable. Thirdly, the diffusion of carriers on the surface of the material accounts for a resolution limit of the photochemical etching; the exact impact of carrier diffusion length on etching resolution will be a key area of investigation in future developments of this technique. All of these factors contribute to broadening and degeneration of the resolvable feature size.

In the next chapter, two novel process integration methods for greatly improved resolutions past the aforementioned limitations will be presented. These innovative integrations will achieve a high-resolution small feature size while maintaining the unique gray-scale capabilities of digital projection photochemical etching.

Chapter 5. Fabrication of High-Resolution Gray-Scale Structures

Considering the issues related with resolution refinement in the previous chapter, it would be greatly beneficial if a high-resolution small pattern size can be achieved while maintaining the novel gray-scale spatial control in the z-axis across the x-y plane. In this chapter, two process integration mechanisms will be explored, allowing the realization of sharper gradients in the etched side-walls together with nanometer-precision variable-depth-control in the vertical axis.

5.1 Integration with Photolithography

Conventional photolithography methods usually achieve a pattern transfer down to sub-micron feature sizes, a great improvement over the current resolution of digital projection photochemical etching. Through spin-coating, exposure, and development of a photoresist (PR) layer on top of the substrate, a resistive layer is formed that outlines the pattern to be protected from the wet etchant. However, one of the major limitations with the orthodox photolithography methods is that only a binary pattern can be defined and etched; the substrate areas not covered with PR will be etched by the wet etchant, whereas the areas shielded by the PR will not, with no intermediate height steps. As such, it will be significantly useful if multiple-level structures can be fabricated in a single etch step with photolithography-defined PR masks. This opens up new opportunities for 3-dimensional device design, boosting the efficiency for the manufacture of multi-level structures and features for semiconductor applications.

Figure 5.1 outlines a conceptual flowchart for the integration of conventional high-resolution lithographical methods with digital projection photochemical etching in the current investigation. Firstly, a bare substrate is patterned with a PR mask delineating the desired etch pattern in Figure 5.1(a)-(b). An image with varied spatial light intensity across the x-y plane is then projected onto the substrate surface in Figure 5.1(c), creating different etch depths across the regions as demonstrated in Figure 5.1(d). Lastly, the PR layer is stripped off and this creates a variable-height ridge array for this example, as shown in Figure 5.1(e). The structure will achieve not only a sharper side-wall gradient from the high-resolution lithographic patterns, but also a variable-height control in the vertical depth from the gray-scale functionality.

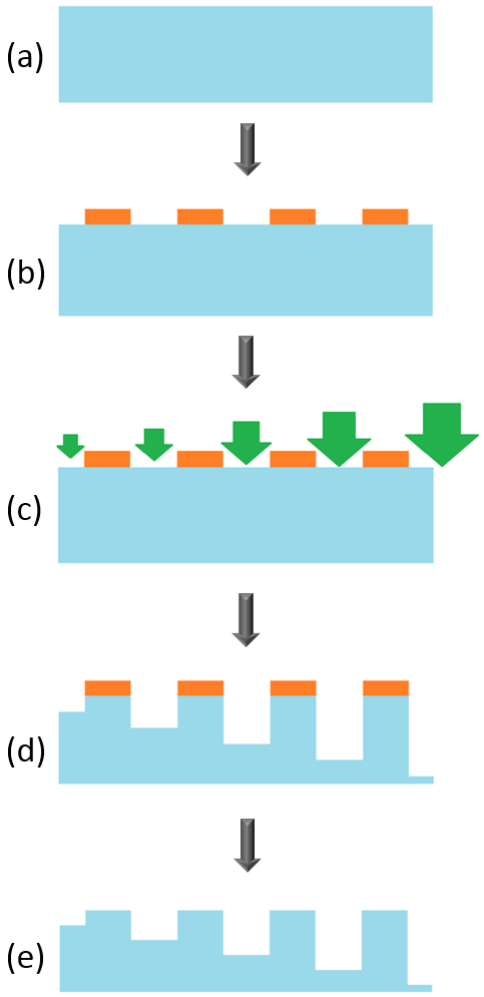

Figure 5.1: Flowchart of the integrated fabrication process combining lithography and digital projection photochemical etching. Blue areas represent the substrate; orange areas represent the PR mask; sizes of the green arrows indicate projected light intensity in each exposed substrate region undergoing wet etching.

In an example to demonstrate the process integration concept, the top-view alignment of the image position on the PR pattern is illustrated in Figure 5.2. The cross-sectional profile of the actual GaAs sample fabricated using the steps outlined in Figure 5.1 is shown in Figure 5.3. PR-covered areas defined the peaks of the four ridges created; five different light intensities were applied in between the ridges, forming five background regions of different depths at approximately 40, 80, 120, 160, and 200 nm respectively. This variable-depth groove array demonstrates the special ability of the integrated fabrication process, in terms of achieving multiple accurately-controlled depths up to nanometer-precision, across the surface on a single substrate sample. In addition, smaller planar patterns in the single-digit-micron range can be defined at each depth/height level, potentially achieving a multi-level 3-

dimensional structure with high-resolution features. More sophisticated patterns beyond this generic example can be created through defining additional patterns using the projected image mask and the PR layer on the substrate.

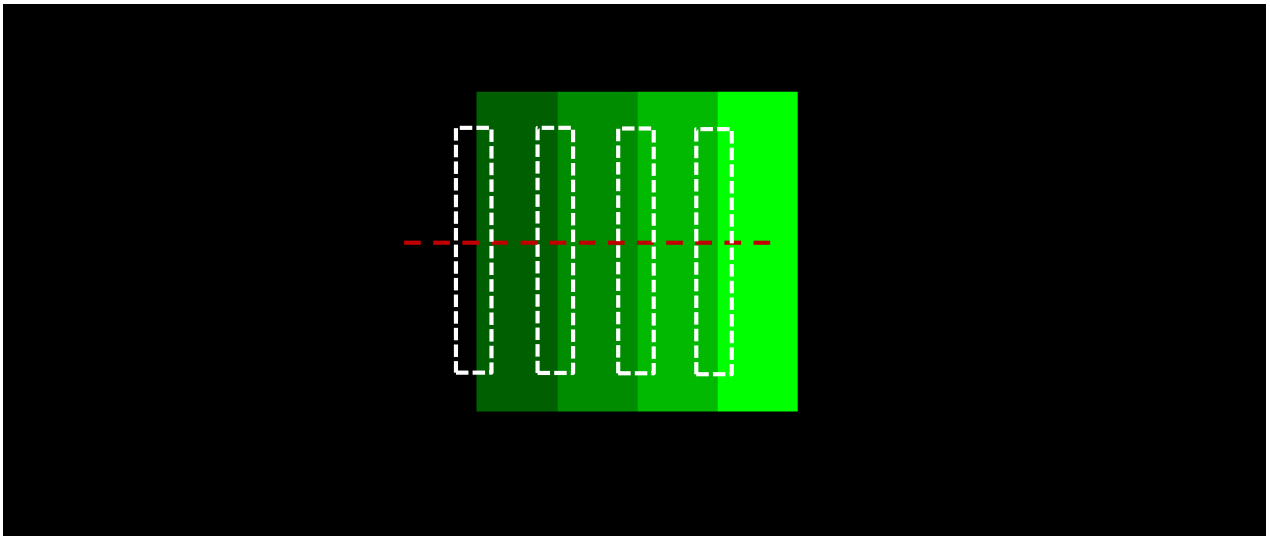

Figure 5.2: The top-view alignment of the projected image mask with respect to PR pattern. The areas enclosed in the white lines are PR-covered regions on the substrate. The red line represents the location of the cross-sectional cut for Figure 5.3.

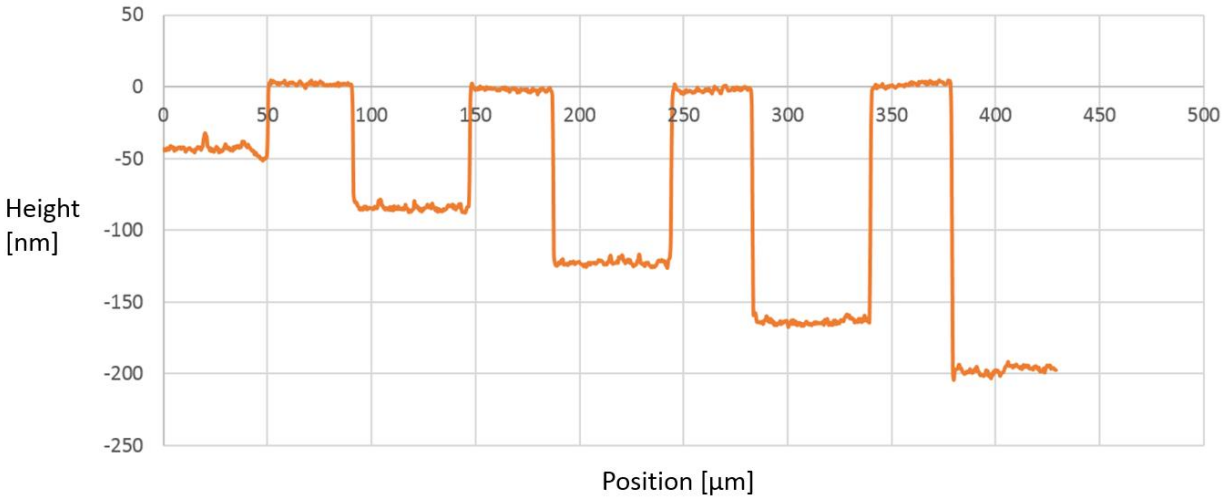

Figure 5.3: Cross-sectional profile of sample fabricated with photolithography and digital projection photochemical etching.

5.2 Integration with E-beam Lithography

In an effort to push the limits of the integration process with digital projection photochemical etching and lithography processes, the next collection of experiments tapped into the electron-beam (e-beam) lithography patterning techniques. Conventional e-beam lithography has been shown to produce feature sizes below 10 nm, making it an ideal candidate to greatly shrink the feature sizes obtainable in a sample [31].

Following the same concept aforementioned in section 5.1, the e-beam patterned sample is etched with a digital image mask comprised of areas with different color intensities. Polymethyl methacrylate (PMMA) is used as the resistive layer, with an array of five USAF-1951 target sets making up the exposed regions on the PMMA pattern. In addition, there are also regions of variable-sized square arrays defined with PMMA on the left and right of the USAF-1951 patterns. Figure 5.4 shows the scanning electron microscopy (SEM) image for parts of the PMMA pattern on the substrate prior to etching, where sub-micron features are evidently resolvable.

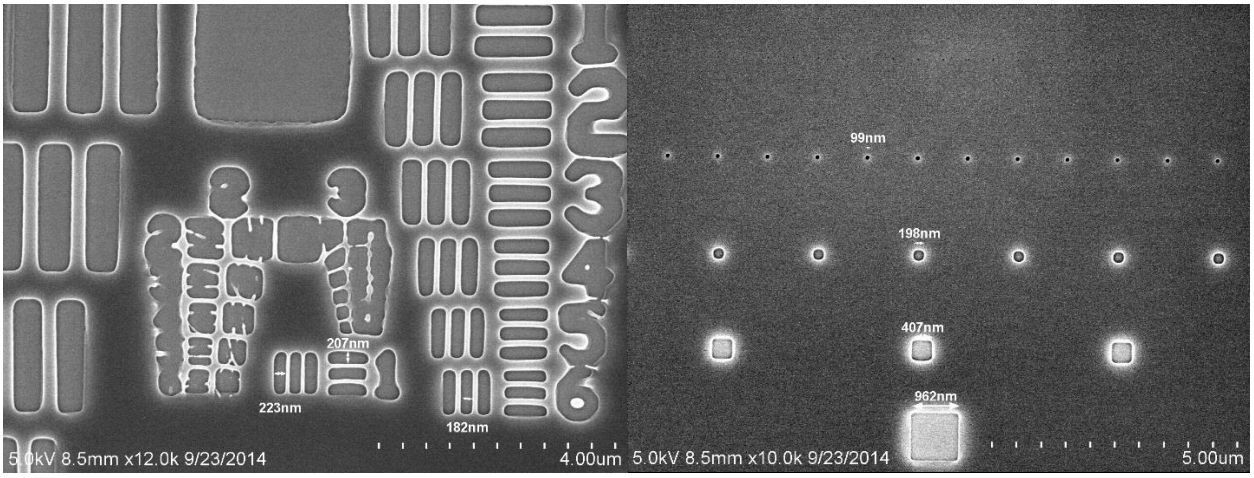

Figure 5.4: SEM images of PMMA-defined sub-micron features on the GaAs substrate using e-beam lithography.

Five different color intensities are respectively projected on the five sets of patterns, achieving a different etch depth for each of the targets. Figure 5.5 displays an optical microscope image of the etched structures; height differences between each set of patterns are clearly visible. More detailed quantitative DPM images are shown in figure 5.6, where distinctive heights for the three USAF-1951 pattern sets can be observed. The other two deeper pattern sets have not been accurately imaged due to depth range

limitations and phase unwrapping issues in the DPM setup. It is also important to recognize that the blurring of smaller patterns in the DPM images in Figure 5.6 is due to the limitations of the imaging technique, and does not accurately portray the high feature resolution of the physical etch patterns on the sample. Considering the nanometer-scale feature sizes in planar surface patterns and vertical depths, integrating digital projection photochemical etching and e-beam lithography has been able to potentially achieve the precise sub-micron feature sizes in all three dimensions.

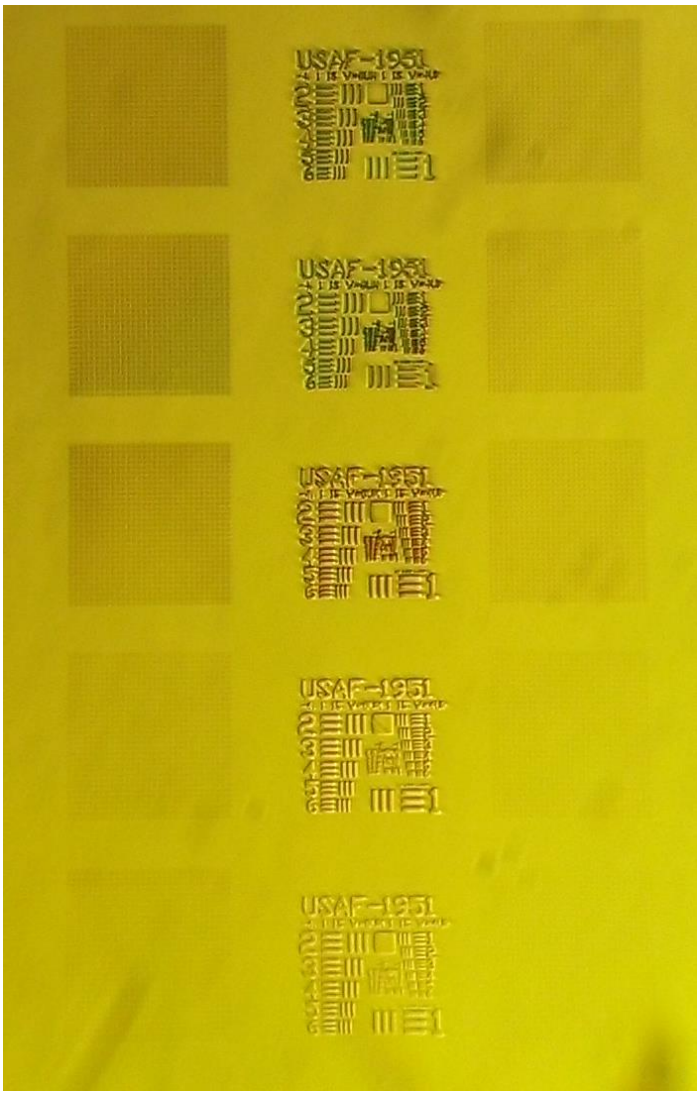

Figure 5.5: Optical microscopy image for the five sets of variable-depth etched patterns defined by sub-micron-resolution e-beam lithography.

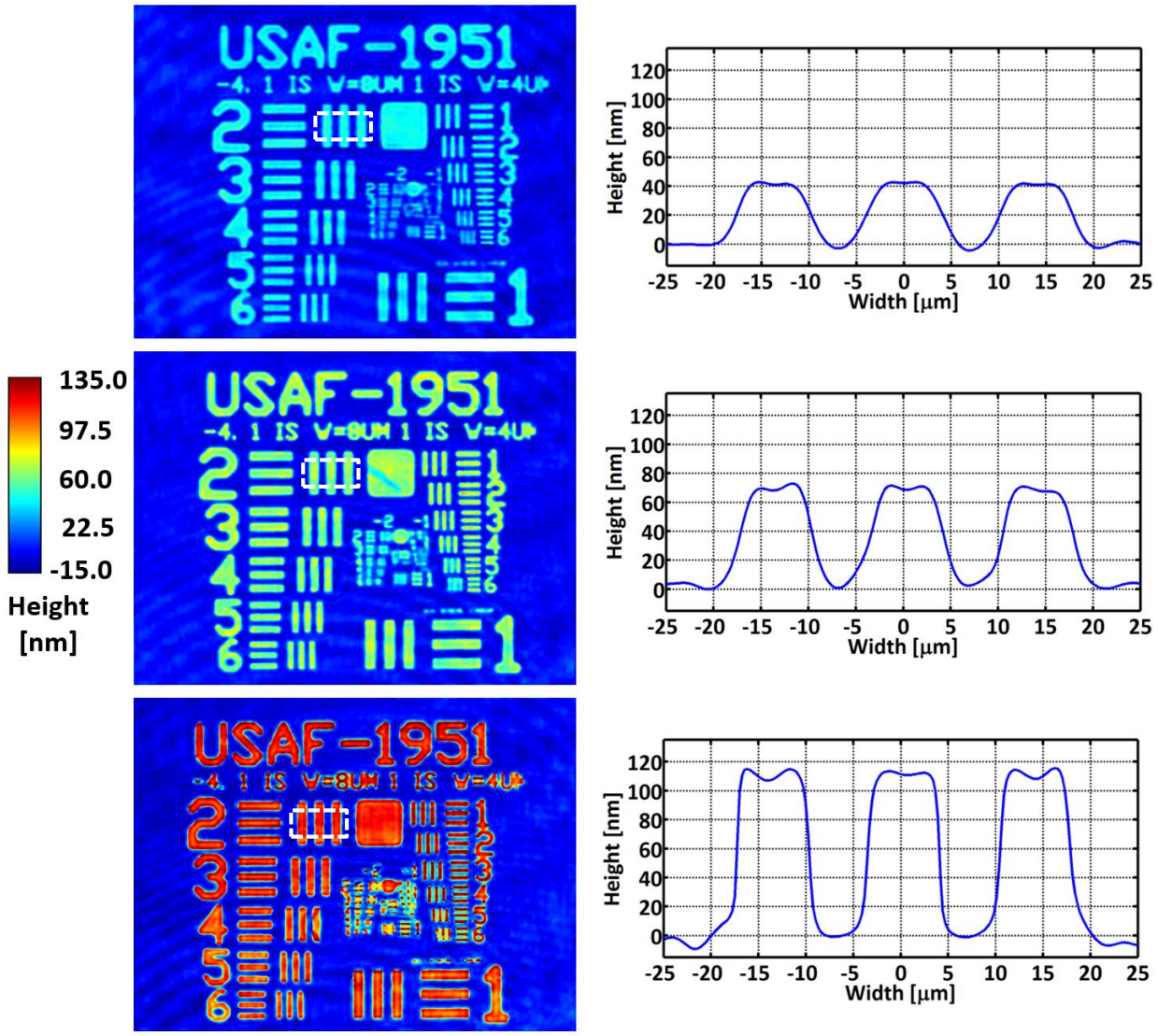

Figure 5.6: DPM images (left) of three variable-height USAF-1951 patterns on the same fabricated GaAs sample as shown in Figure 5.5. The cross-sectional profiles (right) were taken across the areas indicated by the dotted lines.

Chapter 6. Fabrication of Gray-Scale Devices

After documenting the fundamental process parameters and performances for the digital projection photochemical etching, this chapter will explore the fabrication of specific features for functional devices. Three device-specific gray-scale structures are dynamically fabricated and analyzed, demonstrating the simplicity, efficiency, and accuracy of digital projection photochemical etching as an economical fabrication method for MEMS device features.

6.1 Microfluidic Channel for Cell Differentiation

Firstly, a 10-step graduated stair structure is designed for a bioengineering application prototype. This variable-height structure is proposed to function as a microfluidic channel for cell differentiation. As demonstrated in the conceptual schematic of Figure 6.1, a fluid medium containing cells of different sizes will be directed into the channel. The flow direction goes from right to left, up the 10-step micro-stair structure. Depending on the specific size, dimension, and mass of the cells, as well as fluid pressure and flow rate of the liquid medium, the cells will be distributed along the 10 micro-steps at different locations. Larger and heavier cells will settle closer to the lower steps, whereas smaller and lighter cells will be carried further up the set of steps.

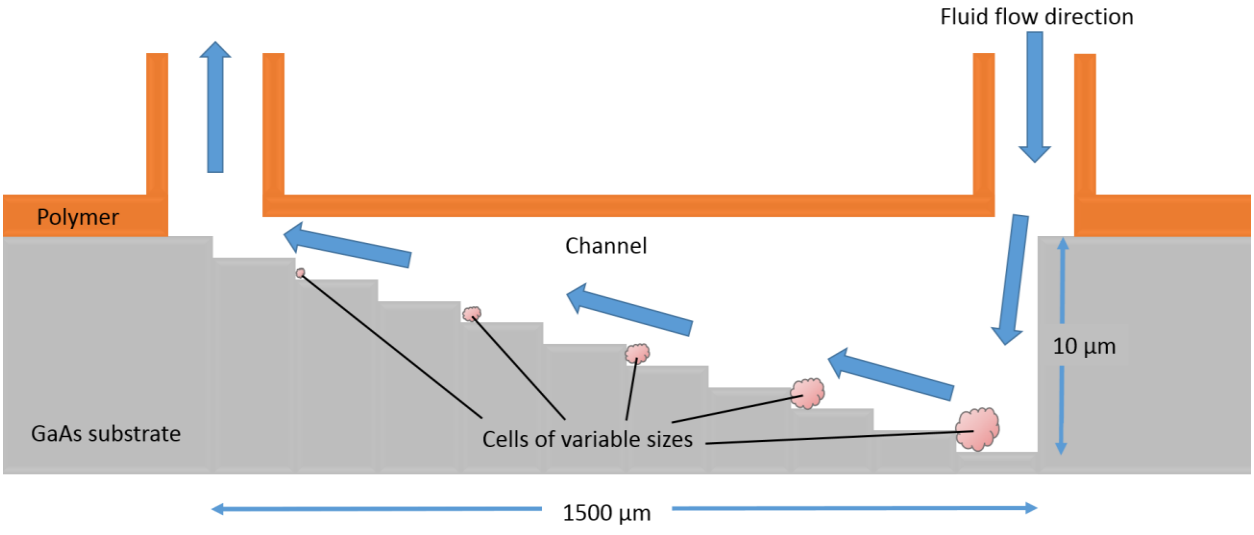

Figure 6.1: Conceptual schematic design for the cell-differentiating microfluidic channel MEMS application.

The depth of the channel is preliminarily designed to be 10 µm at the deepest step, with each step having a depth of 1 µm; the length and width of the channel are designed to be 1500 µm and 800 µm respectively, with each of the 10 steps having a length of 150 µm. In the current research plan, the digital projection photochemical etching will only be utilized for the fabrication of the GaAs part of the channel. The top part of the channel will potentially be constructed using flexible polymers such as polyimide, and will be added after the GaAs multi-step structure has been fabricated.

The actual fabrication of the channel involved a feedback loop of mask design, etching, dimensional analysis, and process adjustment. A multi-frame image mask after a few rounds of iterative modification is shown in Figure 6.2, demonstrating the ability of digital projection photochemical etching to implement dynamic etching processes and enable real-time adjustments to the projected mask during etching.

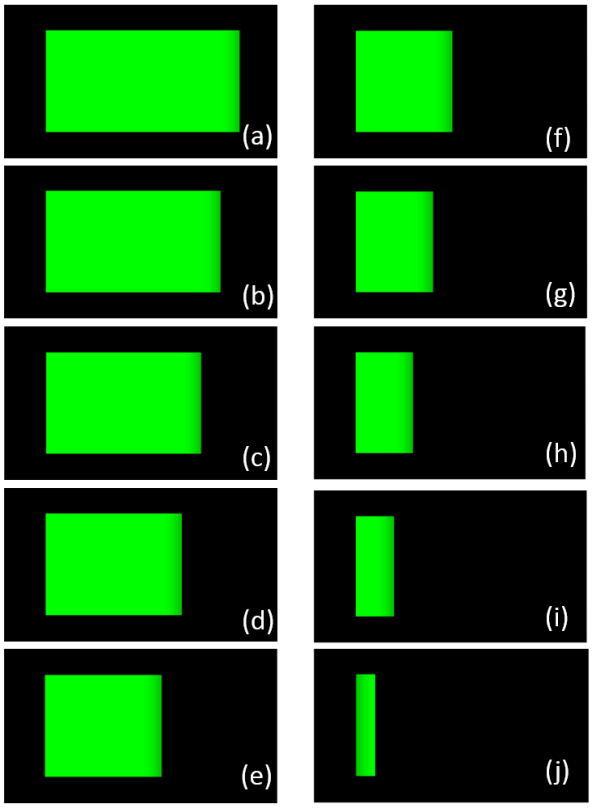

Figure 6.2: A 10-frame dynamic image mask for the 10-step channel structure. Each of the frames (a)-(j) was displayed for 3 minutes in sequence.

The 10-frame mask was displayed for 3 minutes each with a total duration of 30 minutes at room temperature. The green-black boundary on the right side of each frame is responsible for outlining a new step with the differential etch rate across the intensity boundary. There is a slightly pre-warped gradient added near the right side boundary of each green area to counteract a tilt in the fabricated plane, which could be due to uneven diffusion of carriers or geometrical imparities in image focus. Also, note that the actual images focused on the substrate surface will be flipped horizontally due to the reflection from the beam splitter.

The cross-sectional profile of the resulting fabricated structure is presented in Figure 6.3. While the exact dimensions may not match perfectly with the proposed design parameters, it nevertheless demonstrates 10 visible proportionally defined steps with uniform surfaces in most of the intermediate steps. In order to improve the smoothness of the surface topography, it is possible to reduce the etch time through increasing the etch rate. This leads to a shorter etch time which reduces the probability of dust particles and floating impurities entering the etch region, and thus reduces the roughness and granularity on the surface.

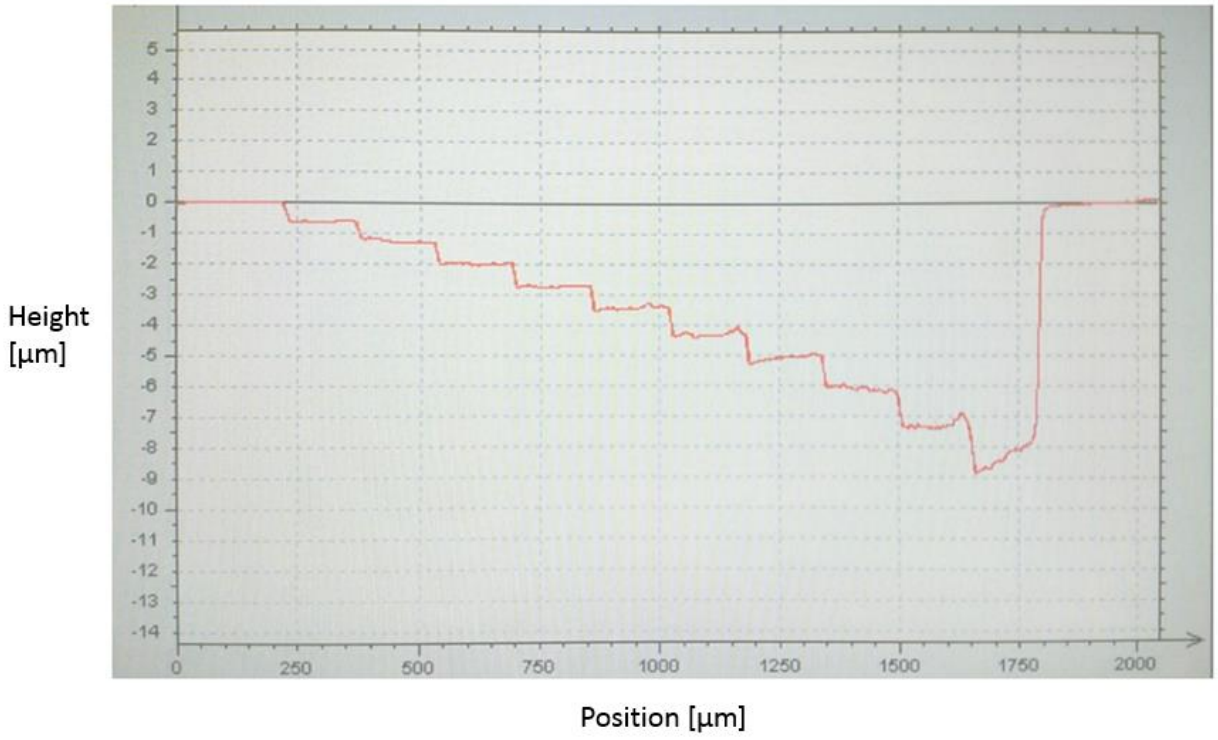

Figure 6.3: Cross-sectional profile of the fabricated GaAs micro-fluidic channel for cell differentiation.

6.2 Variable-Height Pyramid Array for Sensing Applications

In this section, the fabrication of a variable-height pyramid array will be examined. The size of the pyramids was designed to greatly exceed that of conventional semiconductor electronic and photonic devices, and demonstrate gray-scale topographical controls in the depth range as large as 100 μm, which is sometimes found in MEMS actuators. The extreme height of the designed structures requires a much longer etch duration, and a number of other physical controls in terms of image focus. A special mask design was implemented.

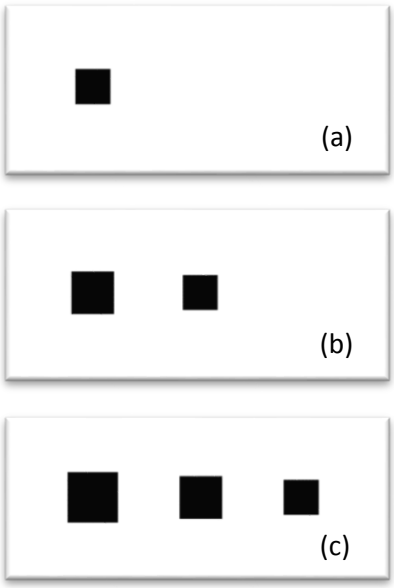

Figure 6.4: The 3-frame image mask used for variable-height pyramid array fabrication. Each of the frames (a)-(c) was displayed sequentially for a total etch time of 3 hours and 10 minutes to obtain the desired heights.

Firstly, in order to maximize the etch rate, a white mask image is used, with a RGB value of 255 in each of the three colors. Part of the projected mask is shown in Figure 6.4; there are three frames which are sequentially projected, with three squares of dynamic sizes displayed at different instances of the etch process, forming three pyramids of different height and sizes. The difference in light intensity between the white and black regions creates the desired differential etch rate. Also, it is important to consider the effect of side-wall etch during the etching process. This will smoothen the side wall of the pyramid and give it its distinctive tilted side walls. In addition, to ameliorate the problem of change in image focus due to the downward etching of the surface, the micrometer stage was controlled using a LabVIEW program to move the sample up at the same rate as the downward etch rate. This maintains the optimal focus of the image exactly at the surface of the GaAs substrate. Lastly, through a trade-off with resolution and light

intensity, the depth of focus for a larger range of focus tolerance is implemented. This is achieved through the attachment of an iris on the beam splitter to reduce the numerical aperture of the optical system.

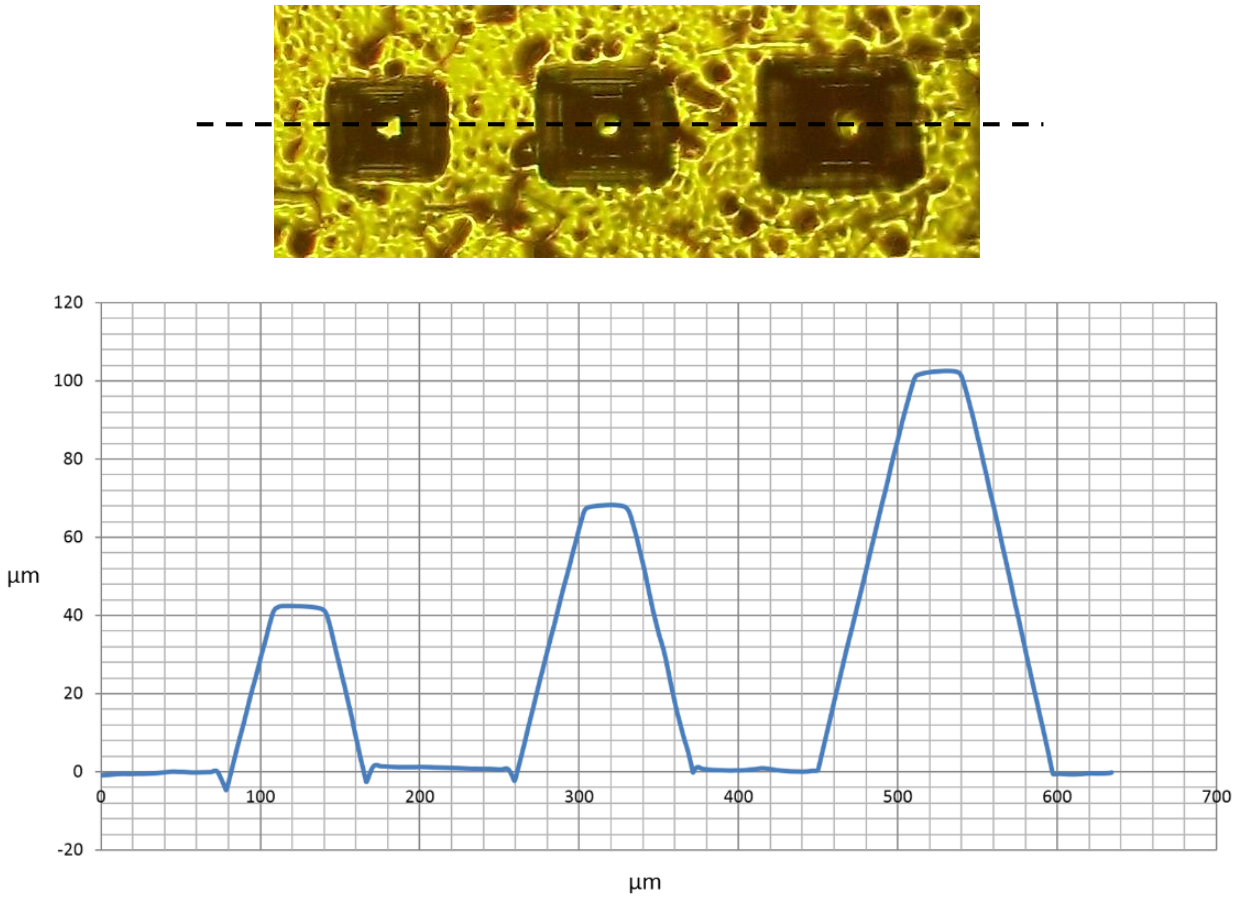

Figure 6.5: Optical microscopy image (top) and cross-sectional profile (bottom) of the fabricated variable-height pyramid array. The cross-sectional profile is taken along the dotted line.

The top-view optical microscopy image and cross-sectional profile of the fabricated pyramid array are shown in Figure 6.5. With the pyramids designed for heights of 40, 70, and 100 µm respectively, an accuracy of within ± 3 µm was achieved. While there are some visible dips at the base of the pyramids, the slopes of the side walls are considerably smooth. A rough granularity can be observed in the background due to extended etch duration, but it is not significant as compared to the height of the pyramid structures.

After demonstrating the substantial range and accuracy of the gray-scale features attainable, some potential applications for the variable-height pyramid array can be considered. One useful MEMS application for pyramidal GaAs structures is as the tip material of the scanning tunneling microscopy (STM), where the properties of GaAs make it well suited as STM-tip material for magneto-optical near-field imaging under ambient conditions [32]. A significant improvement in resolution will have to be achieved before practical tip structures, with width in the range of a few nanometers at the sharpest point, can be fabricated. This application would usually require pyramid base dimensions larger than 5 x 5 μm, which is well within the capabilities of the digital projection photochemical etching technique. As compared to the conventional fabrication method of metal-organic chemical vapor deposition for GaAs pyramidal structures, the digital projection photochemical etching is much more economical and convenient in terms of equipment requirements. In addition, many other promising optical applications could be implemented, such as a pyramid microstructure used on the base of the light guide to replace conventional diffuser dot; a pyramid array made of Si has been used as a micro-mold to replicate patterns on Ni material using an electroforming method [33]. The idea of micro-mold fabrication represents another interesting domain in which the digital projection photochemical etching can be utilized. In addition, a micro-pyramidal-array structure can also be incorporated into quantum well structures for photodetector and solar cell applications [34].

6.3 Waveguide Converter with Vertical Taper

The monolithic integration of several optical elements in the optoelectronic microelectronic system is crucial for the establishment of functional photonic circuitries. In particular, tapered waveguides have been essential in a wide range of optoelectronic devices such as lasers, modulators, and other quantum confined structures in photonic integrated circuits [35]. There is a huge demand for tapered waveguide applications in the fields of optical communications and computing, in which they function as interconnects between multiple optoelectronic components [36].

In this section, a waveguide converter structure with a vertical taper is fabricated with an integrated process of photolithography and digital projection photochemical etching. An array of four narrow ridges acting as waveguides, each with width 5 μm, is fabricated using conventional photolithography and dark wet etching. Subsequently, vertical tapers in the direction of the waveguides are constructed on each of the four waveguides using digital projection photochemical etching. Each

vertical taper is designed to span the horizontal and vertical lengths of 15 µm and 200 nm. Figure 6.6 illustrates the selected area of image mask used and the top-view of the resulting structures formed.

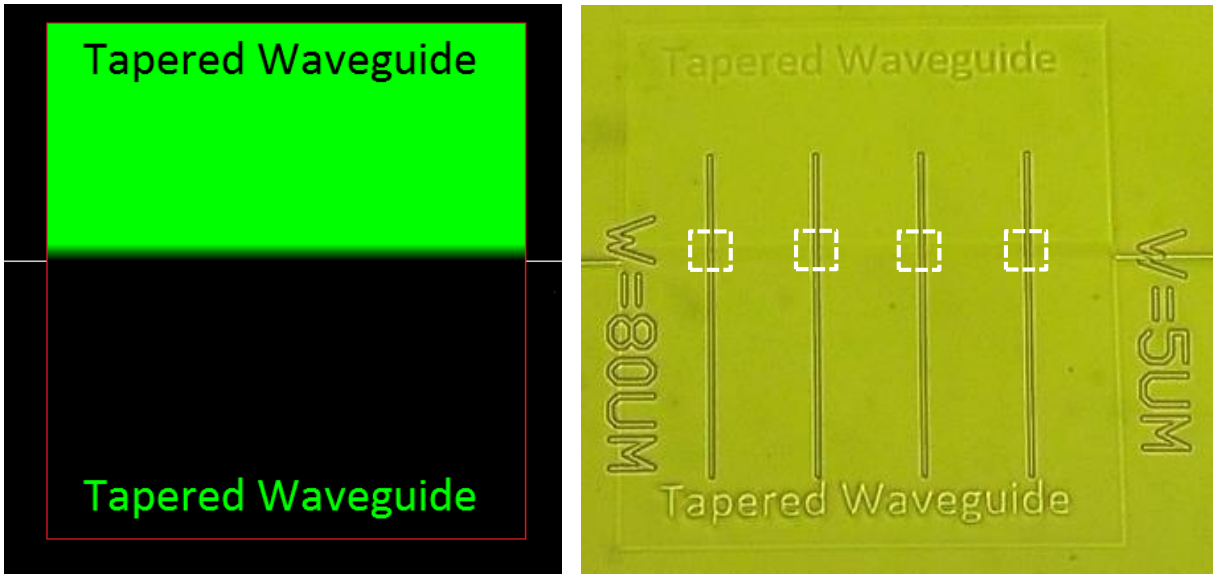

Figure 6.6: Mask image for the tapered waveguide structure (left) and the optical microscopy image of the resulting fabricated sample (right). The dotted lines indicate the tapered region across the four waveguide structures.

With reference to Figure 6.6, the transition from Black to Green-255 occurred over a distance of 11 pixels, representing a tapered region of length 11 pixels x 1.4 µm/pixel ≈ 15 µm. The sample is etched for 20 seconds, which will lead to a differential etch height of approximately 200 nm between the black region and the green region. The taper will be formed on both the waveguide ridges and the background surface around them. Another potential capability of the digital projection photochemical etching is the construction of multiple variable-depth tapers across the same waveguide. An arbitrary depth-control can be easily achieved through the manipulation of spatially-spread color intensities.

A more detailed DPM image of the fabricated tapered waveguide is shown in Figure 6.7. A cross sectional profile of the tapered background region is also plotted. It can be seen that the achieved vertical taper distance is close to the intended value of 200 nm, with a smooth and uniform transition across the tapered region. Also, an improvement to the side-wall angle and structure sharpness could potentially be achieved through performing the photolithographic ridge etch process and the photochemical taper etching in reverse order; a tapered background region could be formed first, followed by photolithography to construct the waveguide patterns across the pre-defined taper. In this case, a conventional wet or dry

etch to form the waveguides will be the last etching step, ideally preserving a better feature sharpness as compared to photochemically etching the taper on pre-constructed waveguides.

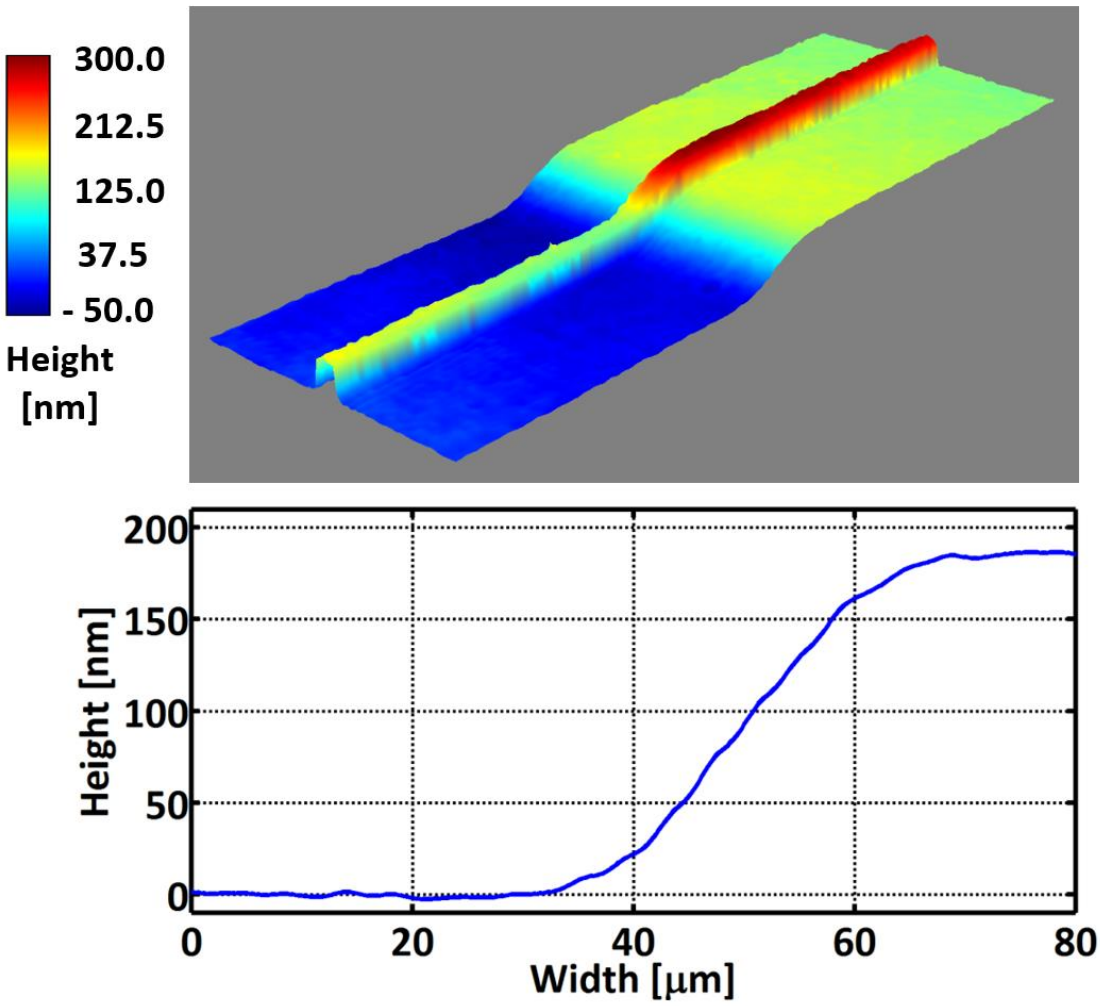

Figure 6.7: DPM image (top) and the cross-sectional plot (bottom) of one of the four tapered waveguide fabricated. The cross-sectional profile is taken along the background, close to the base of the waveguide structure.

The tapered waveguide design shown in Figure 6.7 is analogous to a vertical overlapping waveguide taper transition from a ridge waveguide to a fiber-matched waveguide [37]. Figure 6.8 illustrates such a waveguide taper structure, where the thickness of the upper guiding layer is vertically down-tapered to provide a protruding ridge of constant width and height [37]. As the vertically-guided optical mode in the upper guiding layer reaches the upper edge of the taper, it gradually expands into the thin guiding layers of the diluted fiber-matched structure downwards along the taper. On the other hand,

through a slight modification to this concept, structures similar to an arrayed-waveguide grating with vertically tapered waveguides could potentially be achieved [38]. As such, various applications such as low insertion loss arrayed-waveguide grating could be implemented using an integrated process of photolithography and digital projection photochemical etching.

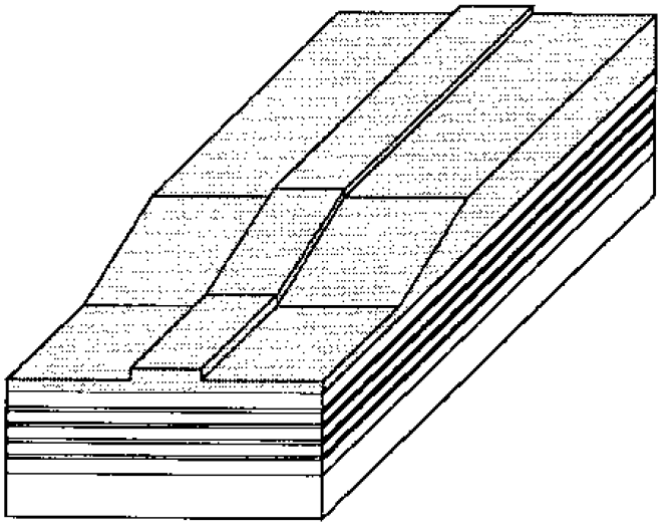

Figure 6.8: Schematic design of the vertical overlapping waveguide taper transition from a ridge waveguide to a fiber-matched waveguide [37].

Chapter 7. Conclusions and Future Work

In light of the above discussion, the performance of the digital projection photochemical etching process was investigated in detail. Numerous characterization tests were carried out and performance parameters of the gray-scale fabrication process for the III-V semiconductor material GaAs were documented. Furthermore, various integration mechanisms with photolithography and e-beam lithography were proposed and implemented, leading to an improvement in feature resolution, aspect ratio, and other dimensional possibilities. Based on the results from the characterization tests, digital image masks were designed for several practical semiconductor device structures. Through the fabrication and analysis of the device features achieved, the range, precision, adaptability, and versatility of the design and fabrication lifecycle were demonstrated. Specifically, the microfluidic channel demonstrates the dynamic, multi-frame digital mask design with pre-warping functionality; the variable height pyramid array displays the accuracy and range for fabricating extremely tall structures, with potential for imaging, optical sensing, and micro-mold fabrication; the waveguide converter exhibits a vertical overlapping waveguide taper which would be useful for a myriad of photonic integrated circuit applications.

Considering the current process performance metrics, there is still room for improvement in terms of resolution, uniformity, and reproducibility. Further modifications and additions could be made to the optical setup, with higher-quality optical elements. For example, the addition of lenses with larger numerical aperture and higher optical power would enable smaller image features to be imaged. A charge-coupled device (CCD) camera could be used to capture the reflected image for automated software control and calibration of the digital mask image.

Conversely, fundamental conceptual modifications such as incorporating immersion lithography and super-continuum laser sources could also drastically improve the specifications of the fabrication process while conserving the present capacities. In addition, it would be useful to explore the specific chemistry behind the light-enabled etching process, optimizing recipes for more semiconductor materials. The oxidation and corrosion of the surface oxide could be separately investigated and controlled, leading to a much more precisely monitored etching process. This would require reconfiguration of the present physical setup and chemical recipes. Some recent results that show nearly infinite light induced etch selectivity with a modified recipe are given in Appendix C.

In conclusion, digital projection photochemical etching, with its distinctive capabilities in gray-scale and maskless fabrication, represents a highly economical and dynamic processing method for

semiconductor materials. With adequate improvements in the near future, it is capable of delivering a wide variety of potential applications in MEMS, optoelectronics, and other 3-dimensional semiconductor applications.

References

[1] Y. Xia and G. M. Whitesides, “Soft lithography,” Annu Rev Mater Sci **28**, 153-184 (1998).

[2] W. Ehrfeld and H. Lehr, “Deep X-ray lithography for the production of three-dimensional microstructures from metals, polymers and ceramics,” Radiat Phys Chem **45**, 349-365 (1995).

[3] S. Y. Chou, P. R. Krauss, and P. J. Renstrom, “Nanoimprint lithography,” J Vac Sci Technol B **14**, 4129 (1996).

[4] B. H. Cumpston, S. P. Ananthavel, S. Barlow, D. L. Dyer, J. E. Ehrlich, L. L. Erskine, A. A. Heikal, S. M. Kuebler, I. Y. Sandy Lee, D. McCord-Maughon, J. Qin, H. Rockel, M. Rumi, X. L. Wu, S. R. Marder, and J. W. Perry, "Two-photon polymerization initiators for three-dimensional optical data storage and microfabrication," Nature **398**, 51-54 (1999).

[5] A. Ostendorf and B. N. Chichkov, “Two-photon polymerization: a new approach to micromachining,” (2006). Available at: http://www.aerotechgmbh.de/media/246109/TwoPhotonPoly.pdf

[6] F. Marty, L. Rousseau, B. Saadany, B. Mercier, O. Francais, Y. Mita, and T. Bourouina, “Advanced etching of silicon based on deep reactive ion etching for silicon high aspect ratio microstructures and three-dimensional micro- and nano structures,” Microelectr J **36**, 673-677 (2005).

[7] S. S. Walavalkar, A. P. Homyk, M. D. Henry, and A. Scherer, “Three-dimensional etching of silicon for the fabrication of low-dimensional and suspended devices,” Nanoscale **5**, 927-931 (2013).

[8] R. Nötzel, “Self-organized growth of quantum-dot structures,” Semicond Sci Technol **11**, 1365-1379 (1996).

[9] C. Edwards, K. Wang, R. Zhou, B. Bhaduri, G. Popescu, and L. Goddard, “Digital projection photochemical etching defines gray-scale features,” Opt Express **21**, 13547-13554 (2013).

[10] C. Edwards, A. Arbabi, G. Popescu, and L. L. Goddard, "Optically monitoring and controlling nanoscale topography during semiconductor etching," Light Sci Appl **1**, e30 (2012).

[11] G. Wysocki, J. Heitz, and D. Bauerle, "Near-field optical nanopatterning of crystalline silicon," Appl Phys Lett **84**, 2025-2027 (2004).

[12] Y. Jung, J. Kim, S. Jang, K. H. Baik, Y. G. Seo, and S. M. Hwang, "Enhanced light extraction of nonpolar a-plane (11-20) GaN light emitting diodes on sapphire substrates by photo-enhanced chemical wet etching," Opt Express **18**, 9728-9732 (2010).

[13] T. D. Lowes and D. T. Cassidy, "Photochemical etching of N-InP as a function of temperature and illumination," J Appl Phys **68**, 814-819 (1990).

[14] M. R. Wang and H. Su, "Laser direct-write gray-level mask and one-step etching for diffractive microlens fabrication," Appl Optics **37**, 7568-7576 (1998).

[15] C. I. H. Ashby and D. R. Myers, “Carrier-lifetime-controlled selective etching process for semiconductors,” (1989). Available at: https://docs.google.com/a/illinois.edu/viewer?url=www.google.com/patents/US5092957.pdf

[16] C.I.H. Ashby, D. R. Myers, and F. L. Vook, “Electronic-carrier-controlled photochemical etching process in semiconductor,” (1989). Available at: https://docs.google.com/a/illinois.edu/viewer?url=www.google.com/patents/US4880493.pdf

[17] S. Terakado, J. Nishino, M. Morigami, M. Harada, S. Suzuki, K. Tanaka, and K. Chikawa, “Photochemical Etching of GaAs using Synchrotron Radiation,” Japan J Appl Phys, Vol. **29**, No.5, pg. 709-711 (1990).

[18] F. Foulon, M. Green, F. N. Goodall, and S. D. Unamuno, “Laser projection patterned etching of GaAs in a chlorine atmosphere,” J Appl Phys **71**, 2898 (1992).

[19] C. I. H. Ashby, “Pattern formation techniques in photochemical etching,” Thin Solid Films **218**, 252-258 (1992).

[20] T. D. Lowes and D. T. Cassidy, “Photochemical etching of n-lnP: Observations on photon efficiency and saturation,” Semicond Sci Technol **8**, 97 (1993).

[21] A. R. Clawson, “Guide to references on III-V semiconductor chemical etching,” Materials Science and Engineering: R: Reports **31**, 1-438 (2001).

[22] H. S. Mavi, S. S. Islam, S. Rath, B. S. Chauhan, and A. K. Shukla, “Laser-induced etching of CrO doped GaAs and wavelength dependent photoluminescence,” Materials Chemistry and Physics **86**, 414-419 (2004).

[23] J. Gao, M. Sailor, S. Bhatia, and C. Flaim, “Direct patterning of silicon by photoelectrochemical etching,” (2005). Available at: https://docs.google.com/a/illinois.edu/viewer?url=patentimages.storage.googleapis.com/pdfs/US20050009374.pdf

[24] T. Simonsmeier, A. Ivankov, and W. Bauhofer, “Sulfidic photochemical passivation of GaAs surfaces in alcoholic solutions,” J Appl Phys **97**, 084910 (2005).

[25] G. Huerta-Cuellar, S. Guel-Sandoval, F. De Anda, V. H. Mendez, B. Torres-Loredo, A. Garnache, A. Joullie, “Photo-selective chemical etching of InAs and GaSb to manufacture microscopic mirrors,” Journal of Applied Electrochemistry **38**, 269-271 (2008).

[26] B. Joshi, S. S. Islam, H. S. Mavi, V. Kumari, T. Islam, A. K. Shukla, and Harsh, “Size-selective laser-induced etching of semi-insulating GaAs: Photoluminescence studies,” Physica E: Low-dimensional Systems and Nanostructures **41**, 690-694 (2009).

[27] M. DeJarld, J. C. Shin, W. Chern, D. Chanda, K. Balasundaram, J. A. Rogers, and X. Li, "Formation of high aspect ratio GaAs nanostructures with metal-assisted chemical etching," Nano Letters **11**, 5259-5263 (2011).

[28] C. A. Edwards, K. Wang, B. G. Griffin, R. Zhou, B. Bhaduri, G. Popescu, and L. L. Goddard, "Fabrication of diffractive optical elements with digital projection photochemical etching," CLEO SI SM1H 4 (2014).

[29] M. P. Sinha and S. Mahapatra, "SEM study of etching of GaAs substrates in the H_3PO_4:H_2O_2:H_2O system," Microelectr J **18**, 48-51 (1987).

[30] A. R. Barron, "Formation of silicon and gallium arsenide wafers," Available at: http://cnx.org/contents/ecf00d82-a47a-47fd-8980-207a74c9f4a9@5/Formation_of_Silicon_and_Galli#eip-965

[31] C. Vieu, F. Carcenac, A. Pepin, Y. Chen, M. Mejias, A. Lebib, L. Manin-Ferlazzo, L. Couraud, and H. Launois, "Electron beam lithography: resolution limits and applications," Appl Surf Sci **164**, 111-117 (2000).

[32] G. J. Bauhuis, P. Mulder, and H. V. Kempen, "Tip formation of micrometer scale GaAs pyramid structures grown by MOCVD," J Cryst Growth **240**, 104-111 (2002).

[33] J. G. Chang, C. W. Liu, W. L. Li, J. M. Lu, and Y. B. Fang, "Fabrication and optical design of a pyramid microstructure for the base of a light guide used in backlight module," J Micro-Nanolith MEM **9**, 043006 (2010).

[34] J. Sun, K. K. Choi, and U. Lee, "Fabrication of pyramidal corrugated quantum well infrared photodetector focal plan arrays by inductively coupled plasma etching with BCl3/Ar," J Micro-Nanolith MEM **11**, 043003 (2012).

[35] F. M. Soares, F. Karouta, E. J. Geluk, J. H. C. V. Zantvoort, H. D. Waardt, and M. K. Smit, "Extremely low-loss vertically-tapered spot size converter in InP-based waveguide structure," Proceedings of the 9th Annual Symposium of the IEEE/LEOS Benelux Chapter, 127-130 (2004).

[36] S. K. Han, "MQW electroabsorption modulator integrated with a tapered waveguide vertical interconnect," J Opt Soc Korea **1**, 44-47 (1997).

[37] I. Moerman, P. P. Van Daele, and P. M. Demeester, "A review on fabrication technologies for the monolithic integration of tapers with III-V semiconductor devices," IEEE J Sel Top Quant **3**, 1308-1320 (1998).

[38] A. Sugita, A. Kaneko, K. Okamoto, M. Itoh, A. Himeno, and Y. Ohmori, "Very low insertion loss arrayed-waveguide grating with vertically tapered waveguides," IEEE Photonic Tech L **12**, 1180-1182 (2000).

Appendix A: Miscellaneous Fabricated Patterns

Prior to the construction of the aforementioned digital projection photochemical etching configuration in Section 3.1.1, a simplified setup is tested. This simplified setup is similar to Figure 3.1, except that there are no optical elements between the Projector and the Cube Beam Splitter. A larger image with higher power intensity if focused onto the GaAs sample surface. Figure A.1 shows the optical microscopy images of two fabricated samples. It can be observed that individual pixels, with a size of approximately 10 µm each, can be individually resolved.

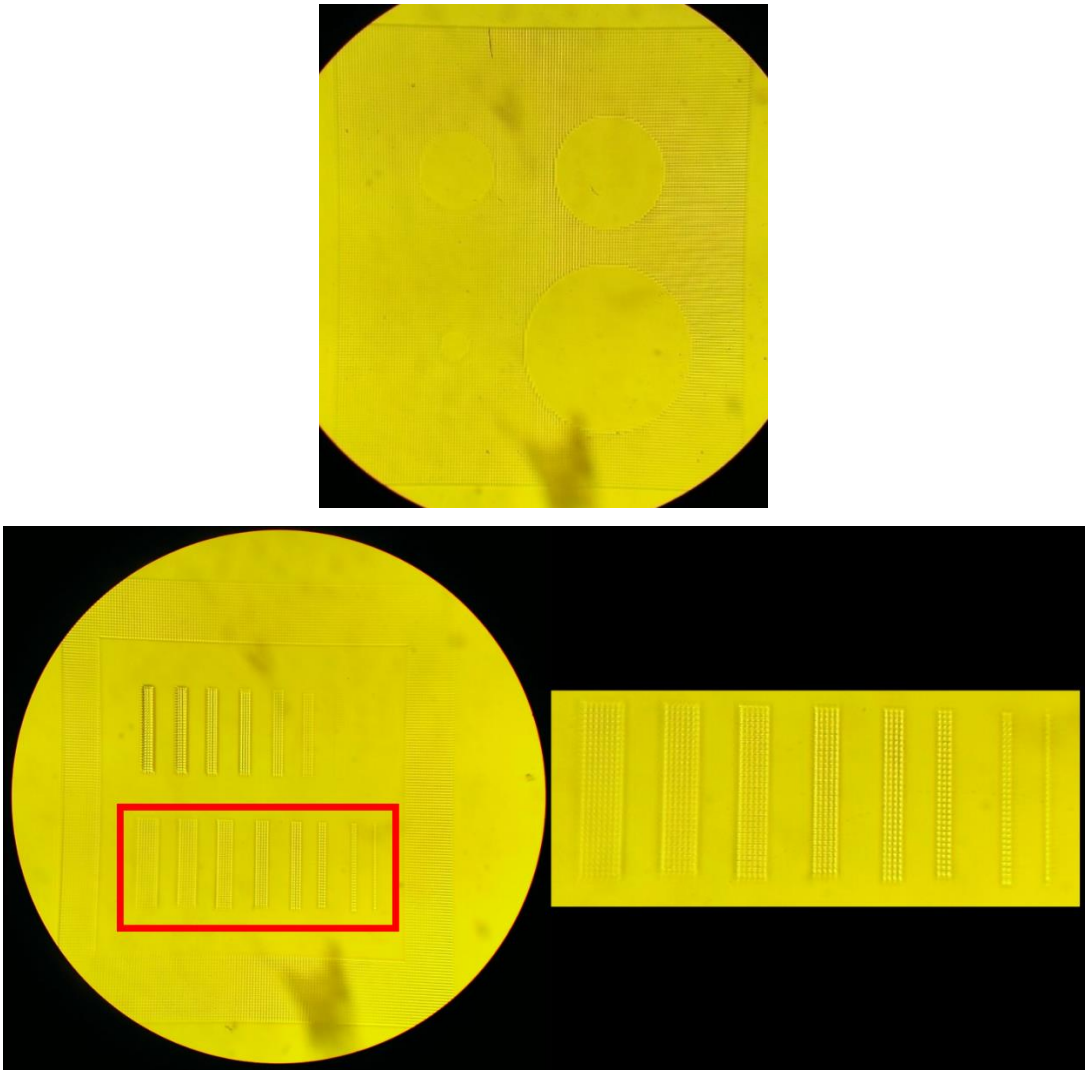

Figure A.1: Optical microscopy images of fabricated GaAs samples from a simplified configuration. The magnified image (bottom right) corresponds to the red-line-enclosed region (bottom left).

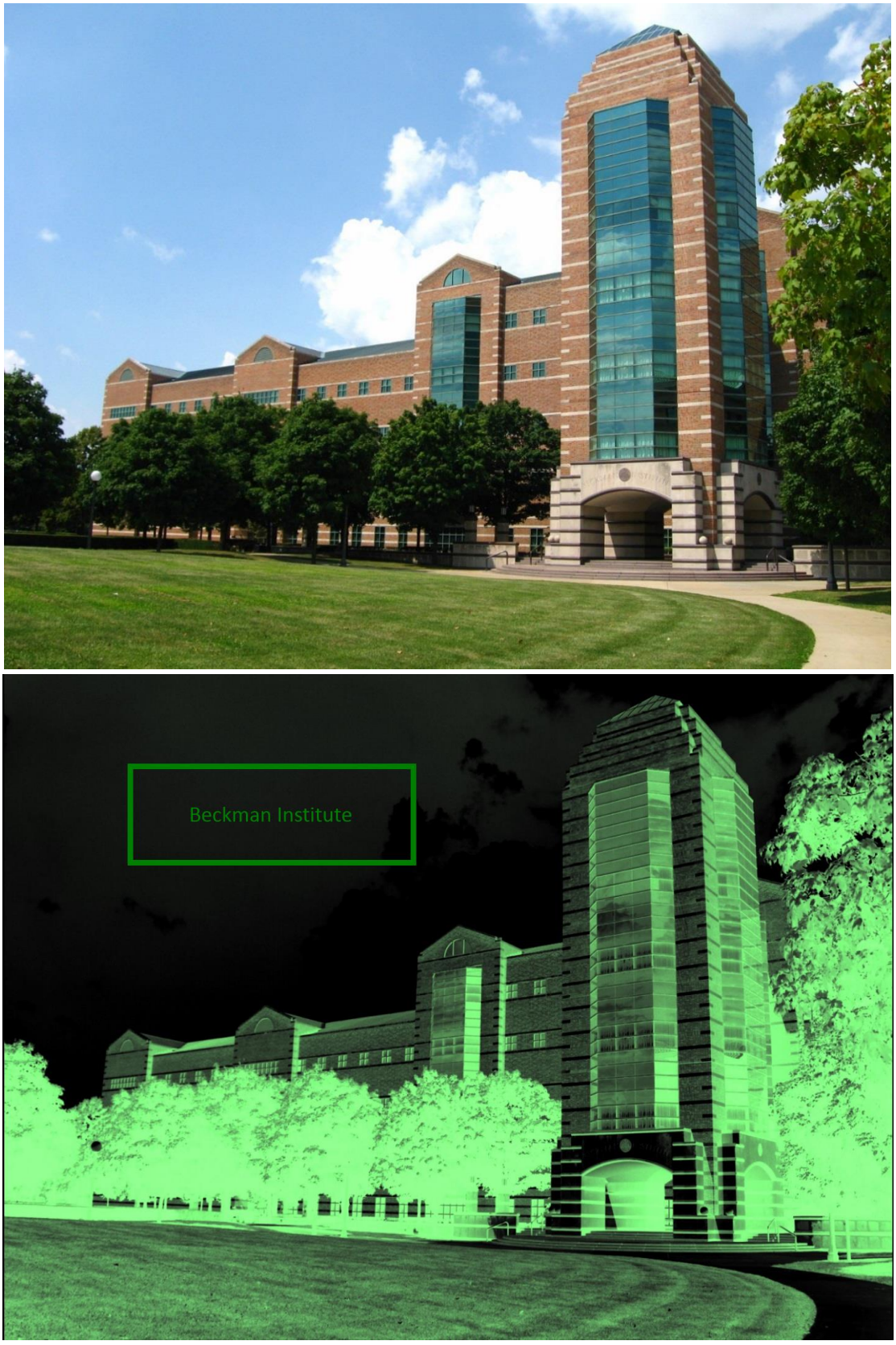

Figure A.2: Unedited digital image and processed image mask used for the fabricated pattern in Figure A.3.

Other than geometrical shapes in manually-designed image masks, arbitrary images were also converted into gray-scale digital masks and used in GaAs sample fabrication. Figure A.2 shows a set of raw image and processed image mask used to fabricate the sample shown in Figure A.3. The image captures the Beckman Institute building from the University of Illinois at Urbana-Champaign.

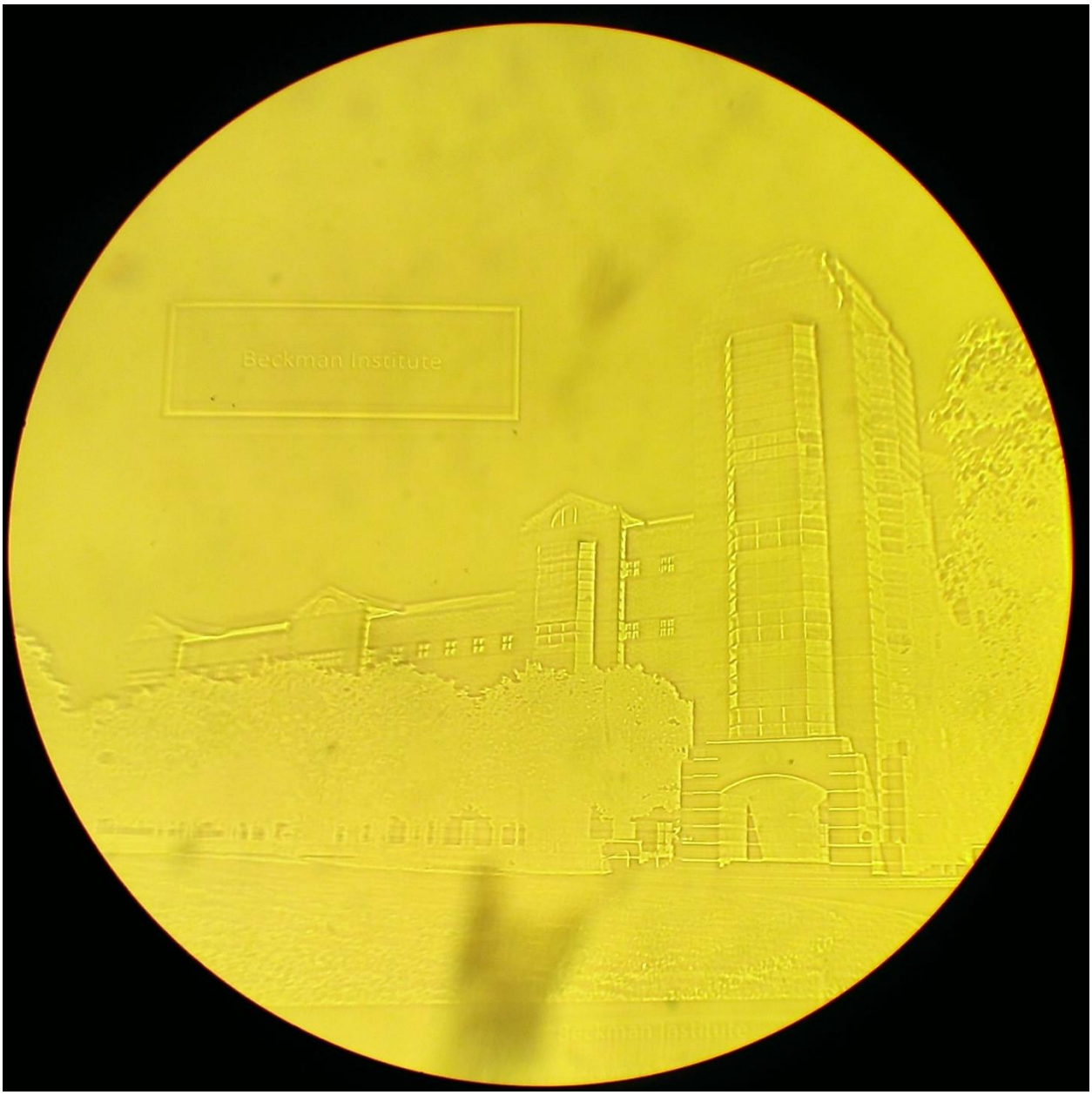

Figure A.3: A GaAs sample fabricated using an edited photo of the Beckman Institute as the mask image.

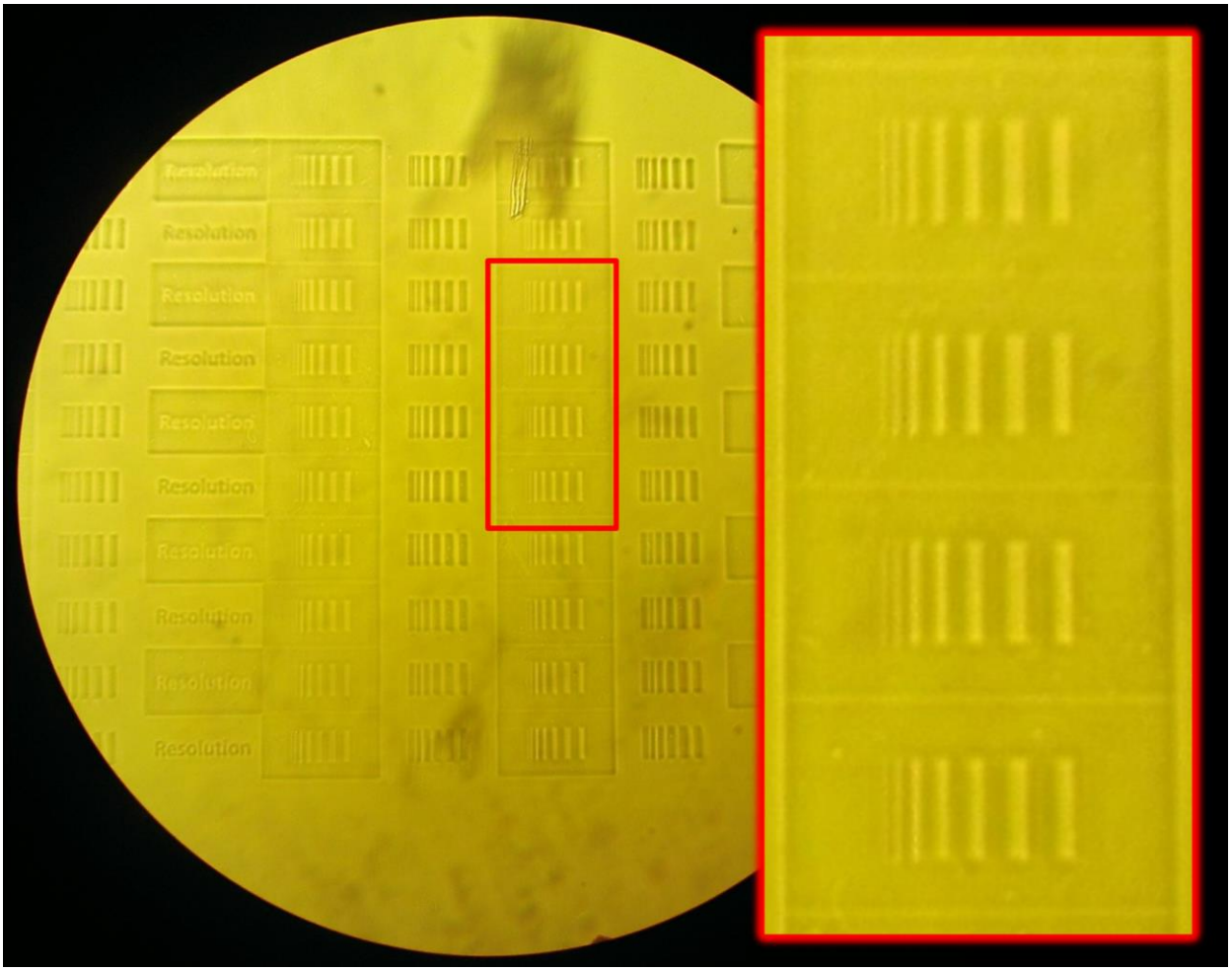

Figure A.4: A GaAs sample fabricated using a set of line arrays of different thicknesses. The red-line-enclosed region is magnified, showing the resolvability of the thinnest lines.

Figure A.4 demonstrates a GaAs sample with numerous sets of line arrays etched. The thinnest optically resolvable line in each array is two pixels or approximately 3 µm wide; this resolution is achieved in both protruding ridges and etched trenches, corresponding to both negative and positive-tone mask regions.

Appendix B: Digital Projection Photoelectrochemical Etching of Si

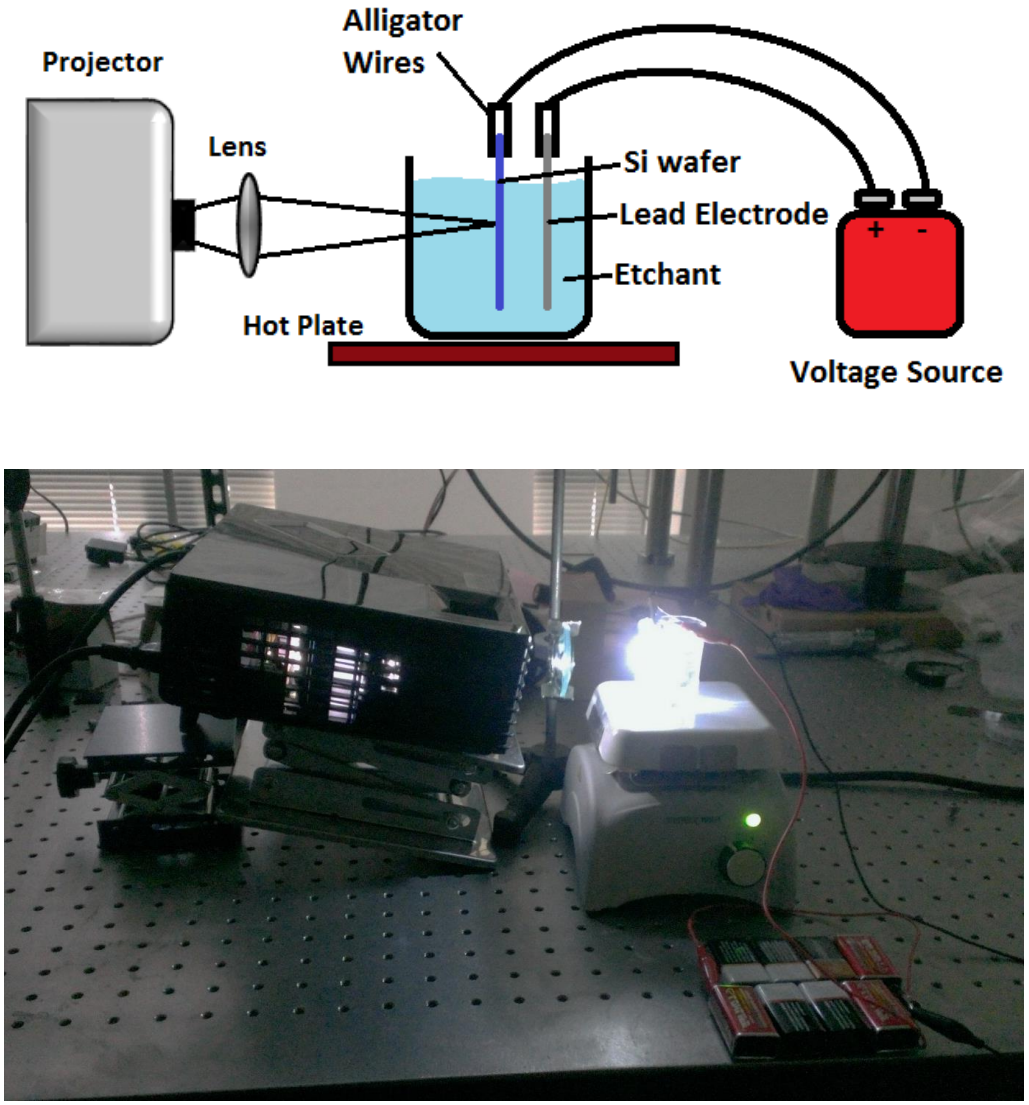

Figure B.1: Schematic design (top) and physical configuration (bottom) of a digital projection photoelectrochemical etching setup specifically for silicon. Mr. Terry Koker of Mahomet-Seymour High School contributed greatly to the design and construction of this setup.

Other than the wide range of tests and fabrication processes implemented on GaAs, there have also been efforts to design a low-cost photoelectrochemical etching setup specifically for silicon. With reference to Figure B.1, a direct-projection mechanism is implemented with the de-magnified projector image focusing directly on a piece of electrically biased p-type (100) silicon wafer. The etchant used is 13:6:1 H_2O:KOH:C_3H_7OH. A temperature of 50^oC is maintained by the hot plate. A cathodic bias of 55V is applied,

with the positive terminal on a lead electrode immersed in the etchant, and the negative terminal applied on the silicon wafer sample.

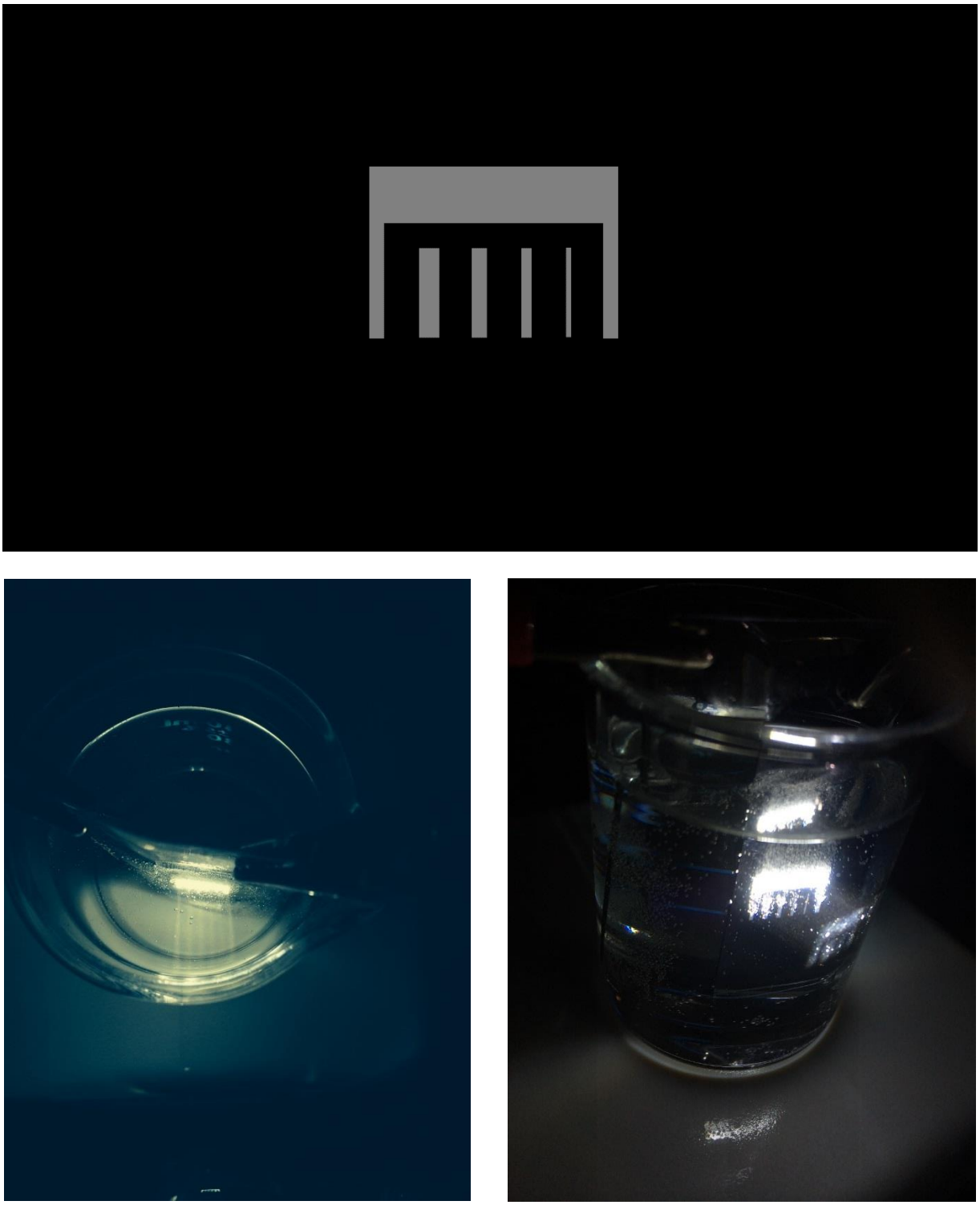

Figure B.2: The mask image (top) used for the etching experiment to characterize resolution, shown in top-view (bottom left) and side-view (bottom right).

A series of photoelectrochemical etching experiments were carried out, demonstrating visible feature sizes as small as 5 mm. Figure B.2 shows the digital mask image and actual experimental setup of a resolution characterization test. One major impediment for achieving smaller resolvable feature sizes is the diffraction of projected light beam due to bubbling of H_2 gas on the sample surface during etching. The 55V applied voltage bias greatly enhances the etch rate, with a very distinct bubbling rate disparity observed before and after the voltage bias is applied. Furthermore, etching experiments with degenerately doped silicon were also conducted. A significant increase in bubbling rate even at lower biased voltages of 9V was observed. The specific etch rate was difficult to quantify due to rough and uneven surfaces.

Appendix C: Digital Projection Photochemical Etching with Citric Acid

In order to strive for better differential etch rates, a new recipe with 1g : 77mL of citric acid monohydrate : H_2O as the etchant was developed. The motivation was to remove H_2O_2 to eliminate the regular chemically induced oxidation step of the reaction and instead have that step solely driven by light. With the new etchant, a negligible dark etch rate was achieved (<3nm for a 20 minute etch) whereas a reasonable light etch rate of 100 nm / 300 sec ≈ 0.33 nm/sec was maintained for White-255. As shown in Figure C.1 and C.2, there is a great disparity in the etch rates for the different regions separately projected with White-255 and Green-128 patterns. This may be due to the expected nonlinearity in the etching rate with light intensity. Since the dark etch rate is essentially zero, sharper side-walls and higher aspect ratio structures can be achieved with this new recipe if carrier diffusion can be minimized.

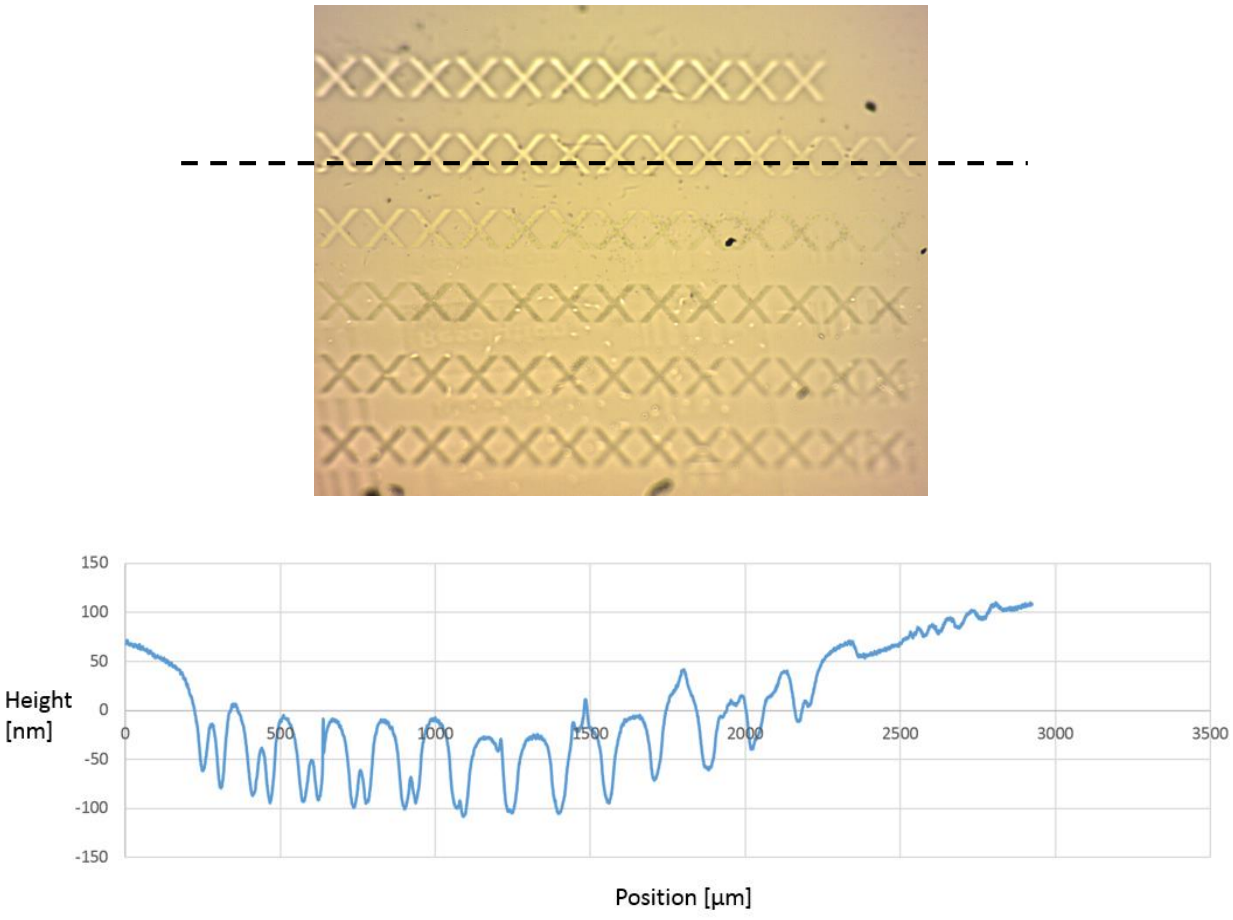

Figure C.1: GaAs sample etched in the citric acid etchant for 5 minutes with a projected array of White-255 crosses (top). The cross sectional profile (bottom) is taken along the dotted line.

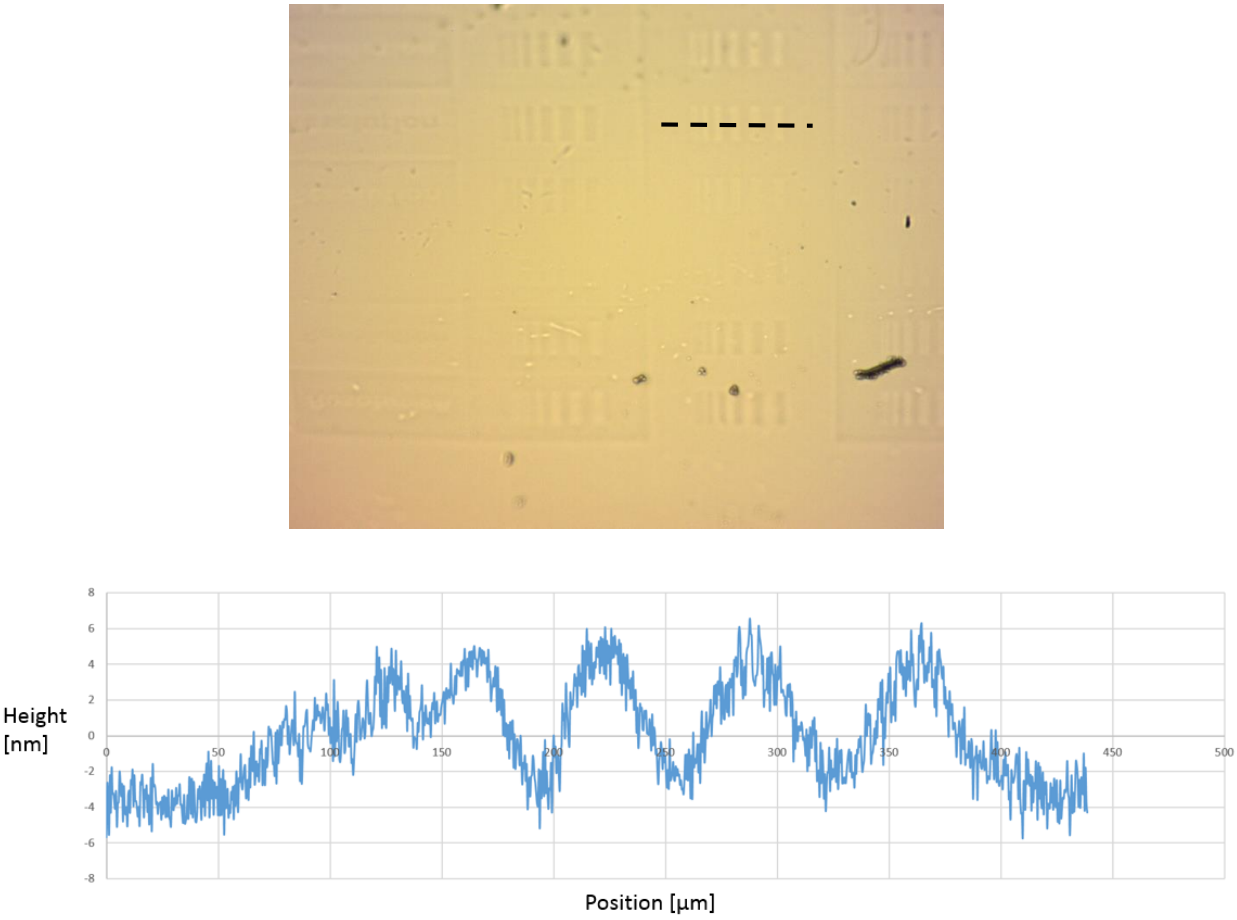

Figure C.2: GaAs sample etched in the citric acid etchant for 10 minutes with a projected array of Green-128 lines (top). The cross sectional profile (bottom) is taken along the dotted line.